Adaptive finite element techniques for the Maxwell equations using implicit a posteriori error estimates

D. Harutyunyan [a,*,2], F. Izsák [a,1], J.J.W. van der Vegt [a,1], M.A. Botchev [a,1]

[a] *Department of Applied Mathematics, University of Twente, P.O. Box 217, 7500 AE Enschede, The Netherlands,*
[d.harutyunyan,f.izsak,j.j.w.vandervegt,m.a.botchev]@math.utwente.nl.

Abstract

We consider an implicit a posteriori error estimation technique for the adaptive solution of the Maxwell equations with Nédélec edge finite element methods on three-dimensional domains. On each element of the tessellation an equation for the error is formulated and solved with a properly chosen local finite element basis. The discrete bilinear form of the local problems is shown to satisfy an inf-sup condition which ensures the well posedness of the error equations. An adaptive solution algorithm is developed based on the obtained error estimates. The performance of the method is tested on various problems including non-convex domains with non-smooth boundaries. The numerical results show that the estimated error, computed by the implicit a posteriori error estimation technique, correlates well with the actual error. On the meshes generated adaptively with the help of the error estimator, the achieved accuracy is higher than on globally refined meshes with comparable number degrees of freedom. Moreover, the rate of the error convergence on the locally adapted meshes is faster than that on the globally refined meshes.

Key words: Maxwell equations, h-adaptive methods, implicit error estimates, Nédélec edge tetrahedral elements

---

* Corresponding author.
[1] This research was supported by the Dutch government through the national program BSIK: knowledge and research capacity, in the ICT project BRICKS (`http://www.bsik-bricks.nl`), Theme MSV1.
[2] Supported by NWO (Netherlands Organization for Scientific Research). Project number 685.000.011.

1 Introduction

In many real life problems (for example, scattering problems, design of optical fibers and antennas, gas and oil exploration) it becomes increasingly important to solve the full set of the Maxwell equations in complex three-dimensional domains. Due to the complexity of the domains, the solution of the Maxwell equations frequently has limited regularity, such as singularities at corners and non-convex edges [17], and efficient solution methods require adaptive techniques in order to capture detailed structures.

A posteriori error estimation techniques to control the adaptation process in finite element methods have become popular tools for the numerical solution of partial differential equations, see e. g. [2,7,8,29,43], and are also important for the Maxwell equations. A crucial requirement for a posteriori error estimation techniques is that they provide an accurate estimate of the error throughout the finite element mesh. The a posteriori error estimate is then used to generate meshes locally finer in areas where the mesh resolution is not sufficient to achieve the required accuracy. For wave type problems as the Maxwell equations, however, since the major part of the computational error arises from boundary singularities, this is possible only if we use a sufficiently fine mesh compared to the wave length. In this case, the major part of the computational error arises from the boundary singularities. Otherwise, when the mesh is not sufficiently fine, the pollution effect can make the a posteriori error estimates unreliable [4] and a further careful analysis is needed to estimate the pollution error separately [5]. There are basically two types of a posteriori error estimation methods, namely explicit and implicit techniques.

Explicit error estimation techniques provide an upper bound for the local error based on the numerical solution (see e. g. [6,7,43]), but generally contain an unknown constant which often is not sharp and do not provide computable error bounds. There are several techniques to obtain explicit bounds for the unknown constant (see e. g. [14]), but in most applications the estimates are somewhat pessimistic, hence the resulting estimators tend to be unrealistic and fail to detect the more subtle nuances of the specific problem. Several applications of adaptive methods with an explicit error estimation technique for the Maxwell equations can be found in [9,11,15,32,33].

Implicit error estimators seek to avoid these disadvantages by retaining the structure of the original equation as much as possible. The idea of implicit a posteriori error estimates is to formulate local problems for the error function, either over a single element or over a small patch of elements, with suitably chosen boundary conditions and then solve them with an appropriate finite element method [1,2]. This technique can provide reliable estimates, but one has to solve additional, small boundary value problems. Beyond the

standard elliptic case these techniques have been applied for flow problems in two-dimensional domains [19] and for the Maxwell equations with a coercive bilinear form [10]. The numerical experiments in [12,31] for the time harmonic Maxwell equations suggest the implicit error estimation technique as a promising approach. Moreover, in [18,34] equilibration techniques have been applied in case of higher order elements, but a precise analysis of this method is still lacking.
In [25,24] we developed an implicit a posteriori error estimation technique for the time harmonic Maxwell equations on a cubic mesh and proved well posedness of the local problems (without any post-processing) with suitably chosen boundary conditions. We also pointed out that this gives a lower bound for the analytic error.

The main goal of this article is to show that the implicit error estimation technique can successfully be applied in an adaptive mesh refinement algorithm. We perform the adaptation on a tetrahedral mesh, which requires some modifications in the analysis compared to [25,24]. As a natural choice for the finite element spaces we use the Nédélec first order edge basis functions of the first type [28]. Then we define a weak formulation for the error equation in each element, which is solved with a finite element method. These local problems are solved with modified second order Nédélec elements where the linear part is removed. The use of higher order elements to solve the local error equations is essential to obtain a good approximation of the error and also reduces the pollution effect discussed in [4,5]. In various test cases (on non-convex domains with singular solutions) we test the performance of the implicit error estimation technique. Provided that the mesh resolution is fine enough we show that the method is capable of detecting regions with a relatively large error and, based on this information and using an adaptive mesh generation technique, we are able to achieve a smaller error on adaptively generated meshes than on globally refined meshes. Also, the reduction of the error using the adaptation procedure based on the implicit error estimation technique is faster than that on globally refined meshes.

An important issue for adaptive methods is how to adapt a mesh while maintaining mesh quality. In particular, it is important to choose a selection algorithm for the subdomains where finer elements are needed. Here we would like to mention that there is no optimal algorithm for marking elements for refinement and several options are discussed in Section 5. For more information about refinement strategies we refer to [3,41,20,35,40]. In all our numerical experiments we use the Centaur mesh generator [16] with so called source based mesh adaptation (see Section 5) depending on the selection of a fixed fraction of elements for refinement. This approach tries to make the local mesh finer in specified regions while preserving the high quality of the mesh. One of the beneficial properties of the Centaur mesh generator is that it avoids elements with large dihedral angles, which is important for achieving accuracy.

This article is organized as follows: in Section 2 we present the Maxwell equations, their weak formulation and define the finite element discretization. Section 3 describes the implicit error estimation technique with a properly chosen local finite element space. The inf-sup condition for the local variational formulation of the error equation is proven in Section 4 using a Poincaré type inequality (Lemma 6). A similar result for quasi uniform subdomains is available in [22], Lemma 4.1. We also investigate the dependence on the frequency of the parameters in the estimates. In Section 5 we discuss several adaptation strategies. The performance of the implicit error estimation technique is investigated for various test cases including non-convex domains in Section 6. Finally, conclusions are drawn in Section 7.

2 Mathematical formalization

Consider the time harmonic Maxwell equations for the electric field $\boldsymbol{E}:\Omega\to\mathbb{R}^3$ with perfectly conducting boundary conditions:

$$\operatorname{curl}\operatorname{curl}\boldsymbol{E} - k^2\boldsymbol{E} = \boldsymbol{J} \quad \text{in } \Omega, \tag{2.1a}$$

$$\boldsymbol{E}\times\boldsymbol{\nu} = 0 \quad \text{on } \partial\Omega, \tag{2.1b}$$

where $\Omega\subset\mathbb{R}^3$ is a Lipschitz domain with outward normal vector $\boldsymbol{\nu}$ and $\boldsymbol{J}\in[L_2(\Omega)]^3$ a given source function. The wave number k relates to the frequency ω and the velocity of the wave propagation c as $k=\frac{\omega}{c}$. The velocity of wave propagation is given as $c=\frac{1}{\sqrt{\varepsilon\mu}}$, where the dielectric permittivity $\varepsilon=\varepsilon_0\varepsilon_r$ and the magnetic permeability $\mu=\mu_0\mu_r$ are material properties. The free space dielectric permittivity and magnetic permeability are defined by $\varepsilon_0=\frac{1}{36\pi}10^{-9}\ \mathrm{Fm}^{-1}$ and $\mu_0=4\pi10^{-7}\ \mathrm{Hm}^{-1}$, respectively [27]. The dimensionless parameters ε_r and μ_r are material dependent and called relative permittivity and relative permeability, respectively.

In this article we consider the dimensionless Maxwell equations to avoid problems with floating point arithmetic when working with very large numbers. For the derivation of the dimensionless Maxwell equations we refer to e. g. [27].

In the subsequent derivations we will need the following Hilbert space corresponding to the Maxwell equations

$$H(\operatorname{curl},\Omega)=\{\boldsymbol{u}\in[L_2(\Omega)]^3:\operatorname{curl}\boldsymbol{u}\in[L_2(\Omega)]^3\},$$

which is equipped with the curl norm

$$\|\boldsymbol{u}\|_{\operatorname{curl},\Omega}=(\|\boldsymbol{u}\|^2_{[L_2(\Omega)]^3}+\|\operatorname{curl}\boldsymbol{u}\|^2_{[L_2(\Omega)]^3})^{1/2}. \tag{2.2}$$

The differential operator curl is understood in a distributional sense. While

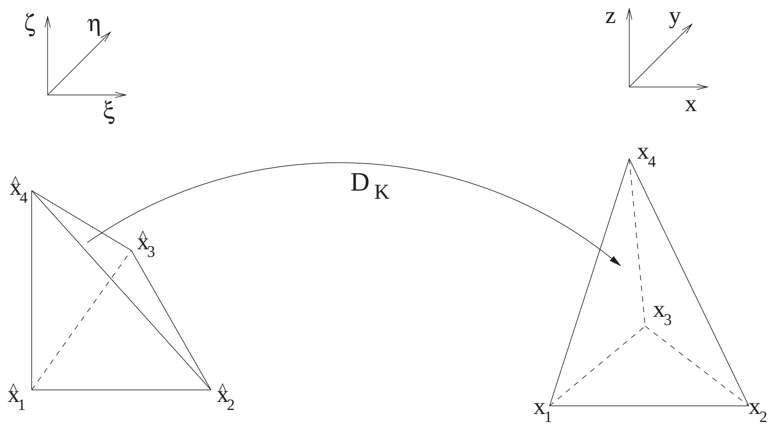

Fig. 1. The reference tetrahedron (left) and tetrahedron in physical space (right).

analyzing (2.1), usually a subspace of $H(\mathrm{curl}, \Omega)$ is used, namely

$$H_0(\mathrm{curl}, \Omega) = \{\boldsymbol{u} \in H(\mathrm{curl}, \Omega) : \boldsymbol{\nu} \times \boldsymbol{u}|_{\partial\Omega} = 0\},$$

where $\boldsymbol{\nu} \times \boldsymbol{u}|_{\partial\Omega}$ denotes the extension of the tangential trace to non smooth functions [27].

For the weak formulation of (2.1) we introduce the following bilinear form

$$B : H(\mathrm{curl}, \Omega) \times H(\mathrm{curl}, \Omega) \to \mathbb{R}$$

with

$$B(\boldsymbol{u}, \boldsymbol{v}) = (\mathrm{curl}\, \boldsymbol{u}, \mathrm{curl}\, \boldsymbol{v}) - k^2(\boldsymbol{u}, \boldsymbol{v}).$$

Similarly, the bilinear form B_K is defined in the same way but now on the subdomain $K \subset \Omega$ (instead of Ω). We will denote by $(\cdot, \cdot)_K$ and $(\cdot, \cdot)_{\partial K}$ the L_2 scalar products on K and ∂K, respectively. In the same way, the curl norm on K is defined by

$$\|\boldsymbol{u}\|_{\mathrm{curl},K} = (\|\boldsymbol{u}\|^2_{[L_2(K)]^3} + \|\mathrm{curl}\, \boldsymbol{u}\|^2_{[L_2(K)]^3})^{1/2}.$$

Using the above notation the weak formulation of the time harmonic Maxwell equations (2.1) is: for a given source function $\boldsymbol{J}$, find $\boldsymbol{E} \in H_0(\mathrm{curl}, \Omega)$ such that for all $\boldsymbol{v} \in H_0(\mathrm{curl}, \Omega)$ the following relation is satisfied

$$B(\boldsymbol{E}, \boldsymbol{v}) = (\boldsymbol{J}, \boldsymbol{v}). \tag{2.3}$$

2.1 Finite elements in $H(\mathrm{curl})$: First order edge elements

For the numerical solution of (2.3) we use the $H(\mathrm{curl})$ conforming edge finite elements proposed by Nédélec [28] for tetrahedral elements.

Table 1

Edge and face enumeration.

Edge #	Node i_1	Node i_2
1	1	2
2	1	3
3	1	4
4	2	3
5	4	2
6	3	4

Face #	Node i_1	Node i_2	Node i_3
1	2	3	4
2	1	3	4
3	1	2	4
4	1	2	3

It is convenient to define the finite elements first on a reference element, which in our case is a tetrahedron $\hat{K}$ with nodes $\hat{X}_1, \hat{X}_2, \hat{X}_3, \hat{X}_4$, see Figure 1, where

$$\hat{X}_1 = (0,0,0),\ \hat{X}_2 = (1,0,0),\ \hat{X}_3 = (0,1,0),\ \hat{X}_4 = (0,0,1).$$

The first order Nédélec elements are defined on the reference element $\hat{K}$ as

$$\boldsymbol{W}_i^0 = (L_{i_1}\nabla L_{i_2} - L_{i_2}\nabla L_{i_1})l_i, \qquad i = 1,\dots,6,$$

where L_j is the Lagrange basis function corresponding to node j of $\hat{K}$, l_i the length of edge i, and i the edge number associated with the nodes i_1 and i_2 (see Table 1). In more explicit form this basis reads

$$\begin{aligned}
&\boldsymbol{W}_1^0 = (1-\eta-\zeta, \xi, \xi)^T\,, && \boldsymbol{W}_2^0 = (\eta, 1-\xi-\zeta, \eta)^T\,,\\
&\boldsymbol{W}_3^0 = (\zeta, \zeta, 1-\xi-\eta)^T\,, && \boldsymbol{W}_4^0 = \sqrt{2}\,(-\eta, \xi, 0)^T\,,\\
&\boldsymbol{W}_5^0 = \sqrt{2}\,(\zeta, 0, -\xi)^T\,, && \boldsymbol{W}_6^0 = \sqrt{2}\,(0, -\zeta, \eta)^T\,,
\end{aligned}$$

with (ξ, η, ζ) denoting the local coordinates on $\hat{K}$.

A detailed construction of Nédélec basis functions can be found, for example, in [27]. Next, we introduce a tetrahedral tessellation $\mathcal{T}_h$ of Ω with N elements and N_e edges. The basis defined on the reference element $\hat{K}$ can be transformed to an arbitrary tetrahedron $K \in \mathcal{T}_h$ using the isoparametric mapping

$$D_K : (\xi,\eta,\zeta) \in \hat{K} \mapsto (x,y,z) = \sum_{i=1}^{4} X_i L_i(\xi,\eta,\zeta) \in K, \tag{2.4}$$

provided that this mapping is a diffeomorphism. Here $X_i = (x_i, y_i, z_i)$ denote the nodes of K. We numerate the nodes in $\hat{K}$ and K such that $X_i = D_K(\hat{X}_i)$.

It is well known that the covariant transformation preserves line integrals under a change of coordinates [27,36], so that the basis functions for a given tetrahedron K can be defined as

$$\boldsymbol{w}_j(x,y,z) = (\mathrm{d}D_K^{-1})^T \boldsymbol{W}_j^0(\xi,\eta,\zeta), \quad j=1,\dots,6, \tag{2.5}$$

where $\mathrm{d}D_K$ is the Jacobian of the transformation D_K.

We denote by W_h the space of Nédélec first order edge basis functions:

$$W_h = \mathrm{span}\left\{\boldsymbol{w}_j(x,y,z) \mid \text{all edges } j=1,\dots,N_e \text{ in } \mathcal{T}_h\right\},$$

where each basis function $\boldsymbol{w}_j(x,y,z)$ is defined with respect to edge j according to (2.5).

Remark 1 *The tangential components of the Nédélec edge basis functions are continuous across the interface of two neighboring elements. Hence, the space* W_h *is a conforming subspace of* $H(curl,\Omega)$*. For details see Lemma 5.35 and the preceding text in [27].*

The discretized version of (2.3) reads:

For given source function $\boldsymbol{J}$, find $\boldsymbol{E}_h \in W_h$, such that for all $\boldsymbol{W} \in W_h$ the following relation is satisfied

$$B(\boldsymbol{E}_h, \boldsymbol{W}) = (\boldsymbol{J}, \boldsymbol{W}). \tag{2.6}$$

3 Implicit error estimation

In this section we formulate the implicit error estimation method to estimate the error in each element of the domain. Also, appropriate local basis functions and boundary conditions are considered for the numerical solution of the local problems.

3.1 Formulation of the local error equation

Assume that $\boldsymbol{E}_h$ is a numerical solution computed using first order Nédélec elements. We aim at estimating the computational error $\boldsymbol{e}_h = (\boldsymbol{E} - \boldsymbol{E}_h)|_K$ on each element $K \in \mathcal{T}_h$, with $\mathcal{T}_h$ being the finite element tessellation. For this we state a variational problem for the local error equation (see [25,24]) on the element K as follows: Find $\boldsymbol{e}_h \in H(\mathrm{curl}, K)$ such that for all $\boldsymbol{v} \in H(\mathrm{curl}, K)$

the following relation is satisfied

$$
\begin{aligned}
B_K(\boldsymbol{e}_h, \boldsymbol{v}) &= (\operatorname{curl} \boldsymbol{e}_h, \operatorname{curl} \boldsymbol{v})_K - k^2(\boldsymbol{e}_h, \boldsymbol{v})_K \\
&= (\operatorname{curl} (\boldsymbol{E} - \boldsymbol{E}_h), \operatorname{curl} \boldsymbol{v})_K - k^2(\boldsymbol{E} - \boldsymbol{E}_h, \boldsymbol{v})_K \qquad (3.1) \\
&= (\operatorname{curl} \boldsymbol{E}, \operatorname{curl} \boldsymbol{v})_K - k^2(\boldsymbol{E}, \boldsymbol{v})_K - ((\operatorname{curl} \boldsymbol{E}_h, \operatorname{curl} \boldsymbol{v})_K - k^2(\boldsymbol{E}_h, \boldsymbol{v})_K) \\
&= (\operatorname{curl}\operatorname{curl} \boldsymbol{E}, \boldsymbol{v})_K - (\boldsymbol{\nu} \times \operatorname{curl} \boldsymbol{E}, \boldsymbol{v})_{\partial K} - k^2(\boldsymbol{E}, \boldsymbol{v})_K - B_K(\boldsymbol{E}_h, \boldsymbol{v})_K \\
&= (\boldsymbol{J}, \boldsymbol{v})_K - (\boldsymbol{\nu} \times \operatorname{curl} \boldsymbol{E}, \boldsymbol{v})_{\partial K} - B_K(\boldsymbol{E}_h, \boldsymbol{v}),
\end{aligned}
$$

where a Green's identity is applied in the fourth line and (2.1a) is used in the last line. In order to get a computable right hand side in (3.1) we use the approximation

$$\boldsymbol{\nu} \times \operatorname{curl} \boldsymbol{E} \approx \boldsymbol{\nu} \times \widetilde{\operatorname{curl} \boldsymbol{E}} \quad \text{on interelement faces,} \qquad (3.2)$$

instead of using the unknown exact value $\boldsymbol{\nu} \times \operatorname{curl} \boldsymbol{E}$. A concrete form of this approximation is given in (3.4). The quantity $\boldsymbol{\nu} \times \operatorname{curl} \boldsymbol{E}$ will henceforth be called the *natural* boundary data. The following variational problem for the error on element K can now be formulated:

For a given source function $\boldsymbol{J}$ and numerical solution $\boldsymbol{E}_h$, find $\hat{\boldsymbol{e}}_h \in H(\operatorname{curl}, K)$ such that for all $\boldsymbol{v} \in H(\operatorname{curl}, K)$ the following relation is satisfied

$$B_K(\hat{\boldsymbol{e}}_h, \boldsymbol{v}) = (\boldsymbol{J}, \boldsymbol{v})_K - (\boldsymbol{\nu} \times \widetilde{\operatorname{curl} \boldsymbol{E}}, \boldsymbol{v})_{\partial K} - B_K(\boldsymbol{E}_h, \boldsymbol{v}). \qquad (3.3)$$

3.2 Numerical solution of the local error equation

We will now give a discretized form of the local problem (3.3) which requires a specific choice for the approximation (3.2) of the natural boundary conditions and the finite element basis on element K.

3.2.1 Approximation of the natural boundary conditions

We first specify the approximation in (3.2). We introduce f_j, the common face of the two neighboring elements K and K_j, and $\boldsymbol{\nu}_j$ the outward normal on f_j with respect to K. We approximate $\boldsymbol{\nu} \times \operatorname{curl} \boldsymbol{E}$ on f_j with the average of the tangential traces of the curl of the numerical approximation $\boldsymbol{E}_h$ on its two sides K and K_j. That is we shall use the approximation

$$\boldsymbol{\nu}_j \times \operatorname{curl} \boldsymbol{E}|_{f_j} \approx \frac{1}{2}(\boldsymbol{\nu}_j \times \left[\operatorname{curl} \boldsymbol{E}_h|_{\partial K \cap f_j} + \operatorname{curl} \boldsymbol{E}_h|_{\partial K_j \cap f_j}\right]), \qquad (3.4)$$

which can be straightforwardly implemented.

Suppose that element K intersects with a portion of the boundary of the domain Ω where perfectly conducting boundary conditions are imposed. If K has at least one face on $\partial\Omega$, we impose

$$\boldsymbol{\nu} \times \hat{\boldsymbol{e}}_h = 0 \text{ on } \partial K \cap \partial\Omega. \tag{3.5}$$

Here, it is assumed that the finite element approximation has been constructed so that the perfectly conducting boundary conditions are satisfied exactly, for details see [2].

3.2.2 Choice of the local basis

As discussed in [2], Section 3.4.2, the finite dimensional space used to discretize the local error equations (3.3) has to be selected carefully. In case of elliptic boundary value problems a different local basis is considered in [2] for the solution of the local error equations. It is advocated there that the use of different basis functions than those used for the original problem might result in a better approximation of the error. For the Maxwell equations it is also beneficial to use higher order polynomials for the error equation which is explained by the fact that the dominant term in the error is associated with polynomials of a degree which is one order higher than those used to approximate the field, see [12,31,34]. In our numerical experiments we observe similar phenomena. If we use the first order Nédélec elements to solve the local problems then the computed error does not describe the true error and leads to a non-physical solution. If we use the full second order Nédélec elements again the obtained results are poor, see Section 6.4. This is due to the linear part present in the basis. Therefore, as a basis for the solution of the local error equations, we use the second order Nédélec edge basis functions with the linear basis functions removed.

Again, the basis functions for the local problem are first defined on a reference tetrahedron and then with the covariant transformation (2.5) transformed to the physical elements. There are eight face based basis functions defined as

$$\begin{aligned}
\boldsymbol{\phi}_1^0 &= L_2L_3\nabla L_4 - L_2L_4\nabla L_3, & \boldsymbol{\phi}_2^0 &= L_2L_3\nabla L_4 - L_3L_4\nabla L_2,\\
\boldsymbol{\phi}_3^0 &= L_1L_3\nabla L_4 - L_1L_4\nabla L_3, & \boldsymbol{\phi}_4^0 &= L_1L_3\nabla L_4 - L_3L_4\nabla L_1,\\
\boldsymbol{\phi}_5^0 &= L_1L_2\nabla L_4 - L_1L_4\nabla L_2, & \boldsymbol{\phi}_6^0 &= L_1L_2\nabla L_4 - L_2L_4\nabla L_1,\\
\boldsymbol{\phi}_7^0 &= L_1L_2\nabla L_3 - L_1L_3\nabla L_2, & \boldsymbol{\phi}_8^0 &= L_1L_2\nabla L_3 - L_2L_3\nabla L_1,
\end{aligned}$$

or, in more explicit form,

$$
\begin{aligned}
\boldsymbol{\phi}_1^0 &= (0, -\xi\zeta, \xi\eta)^T\,, & \boldsymbol{\phi}_2^0 &= (-\eta\zeta, 0, \xi\eta)^T\,,\\
\boldsymbol{\phi}_3^0 &= (0, -(1-\xi-\eta-\zeta)\zeta, (1-\xi-\eta-\zeta)\eta)^T\,, & \boldsymbol{\phi}_4^0 &= (\eta\zeta, \eta\zeta, (1-\xi-\eta)\eta)^T\,,\\
\boldsymbol{\phi}_5^0 &= (-(1-\xi-\eta-\zeta)\zeta, 0, (1-\xi-\eta-\zeta)\xi)^T\,, & \boldsymbol{\phi}_6^0 &= (\xi\zeta, \xi\zeta, (1-\xi-\eta)\xi)^T\,,\\
\boldsymbol{\phi}_7^0 &= (\eta(1-\xi-\eta-\zeta), \xi(1-\xi-\eta-\zeta), 0)^T\,, & \boldsymbol{\phi}_8^0 &= (\xi\eta, (1-\xi-\zeta)\xi, \xi\eta)^T\,.
\end{aligned}
$$

These basis functions are transformed to a tetrahedron $K \in \mathcal{T}_h$ with the covariant transformation as

$$
\boldsymbol{\phi}_j(x, y, z) = (\mathrm{d}D_K^{-1})^T \boldsymbol{\phi}_j^0(\xi, \eta, \zeta), \quad j = 1, \ldots, 8, \tag{3.6}
$$

with D_K being the transformation defined in (2.4). This reduced finite element space on an element K is denoted by $\mathcal{N}_2^2(K)$:

$$
\mathcal{N}_2^2(K) = \mathrm{span}\{\boldsymbol{\phi}_j\}_{j=1,\ldots,8}.
$$

For more details on the construction of second order Nédélec elements we refer to [27,38].

3.2.3 Weak form of the local error equation

Using approximation (3.4) and the local basis $\mathcal{N}_2^2(K)$ we obtain the discrete form of the local error equation (3.3):

For a given source function $\boldsymbol{J}$ and numerical solution $\boldsymbol{E}_h$, find $\hat{\boldsymbol{e}}_h \in \mathcal{N}_2^2(K)$ such that for all $\boldsymbol{w} \in \mathcal{N}_2^2(K)$ the following relation is satisfied

$$
\begin{aligned}
(\mathrm{curl}\, \hat{\boldsymbol{e}}_h, \mathrm{curl}\, \boldsymbol{w})_K - k^2(\hat{\boldsymbol{e}}_h, \boldsymbol{w})_K &= (\boldsymbol{J}, \boldsymbol{w})_K - (\mathrm{curl}\, \boldsymbol{E}_h, \mathrm{curl}\, \boldsymbol{w})_K\\
&\quad + k^2(\boldsymbol{E}_h, \boldsymbol{w})_K - \frac{1}{2}(\boldsymbol{\nu}_j \times \left(\mathrm{curl}\, \boldsymbol{E}_h|_K + \mathrm{curl}\, \boldsymbol{E}_h|_{K_j}\right), \boldsymbol{w})_{\partial K},
\end{aligned} \tag{3.7}
$$

with suitable modification if there is at least one face in $\partial K \cap \partial\Omega$.

3.3 Properties of the local error estimator

We investigate the existence and uniqueness of the local error approximation $\hat{\boldsymbol{e}}_h$ and state that it provides a lower bound (up to a constant) for the exact error $\boldsymbol{e}_h$.

3.3.1 Well posedness of the local error equation

Using a lifting operator we can associate an $\bar{\boldsymbol{e}}_h$ to $\hat{\boldsymbol{e}}_h$ and define a function $\hat{\boldsymbol{J}}_K \in [L_2(\Omega)]^3$ such that the well posedness of (3.3) is equivalent with that of the variational problem: Find an $\bar{\boldsymbol{e}}_h \in H(\mathrm{curl}, K)$ such that for all $\boldsymbol{v} \in H(\mathrm{curl}, K)$ the following relation is satisfied

$$B_K(\bar{\boldsymbol{e}}_h, \boldsymbol{v}) = (\hat{\boldsymbol{J}}_K, \boldsymbol{v}). \tag{3.8}$$

For the details we refer to [25,24], Section 3.3.1.

The well posedness of (3.8) is stated in the following:

Lemma 2 *Assume that k is not a Maxwell eigenvalue on K in the sense that only $\boldsymbol{u} = 0 \in H(\mathrm{curl}, K)$ satisfies the relation*

$$B_K(\boldsymbol{u}, \boldsymbol{v}) = 0, \ \forall \boldsymbol{v} \in H(\mathrm{curl}, K).$$

Then the variational problem (3.8) *has a unique solution.*

For the proof we refer to [25,24], Section 3.3.3.

In order to apply Lemma 2 we need to ensure that k is not a Maxwell eigenvalue on K for all kind of tetrahedra arising in the finite element tessellation $\mathcal{T}_h$. Instead of performing a detailed analysis for this, we rather ensure well posedness for the discretized problems in (3.8) by proving an inf-sup condition, which is discussed in Section 4.

3.3.2 Efficiency of the local error estimate

We state that the error estimate $\hat{\boldsymbol{e}}_h$ is efficient which means that it is bounded by the analytic error plus higher order terms (for a precise definition see [13]). For this we use the notation:

$$\boldsymbol{r}_K = \boldsymbol{J} - \mathrm{curl}\,\mathrm{curl}\,\boldsymbol{E}_h + k^2 \boldsymbol{E}_h \quad \text{in } K$$

for the residual within the subdomain K and

$$\boldsymbol{R}_{l_j} = \frac{1}{2}(\boldsymbol{\nu}_j \times \left[\mathrm{curl}\,\boldsymbol{E}_h|_K - \mathrm{curl}\,\boldsymbol{E}_h|_{K_j}\right])$$

for the tangential jump of the curl at the common face l_j of K and K_j. We also introduce $\bar{\boldsymbol{r}}$ as the approximation of $\boldsymbol{r}$ in the finite element space $\mathcal{N}_2^2(K)$. Similarly, $\bar{\boldsymbol{R}}$ denotes the approximation of $\boldsymbol{R}$ on ∂K with the trace of functions in $\mathcal{N}_2^2(K)$ and the patch $\tilde{K}$ of K is defined as follows:

$$\tilde{K} = \{\cup K_i : K_i \in \mathcal{T}_h, \overline{K} \cap \overline{K}_i \neq \emptyset\}.$$

Theorem 3 *If* $\operatorname{diam} K = h < \frac{h_*}{k}$ *for some positive constant* h_* *then the error estimate* $\hat{\mathbf{e}}_h$ *is efficient,*

$$\|\hat{\boldsymbol{e}}_h\|^2_{\mathrm{curl},K} \le C((1+k^2)^2\|\boldsymbol{e}_h\|^2_{\mathrm{curl},\tilde{K}} + h^2\|\bar{\boldsymbol{r}} - \boldsymbol{r}\|^2_{[L_2(K)]^3} + h\|\bar{\boldsymbol{R}} - \boldsymbol{R}\|^2_{[L_2(\partial K)]^3}), \tag{3.9}$$

where C *does not depend on* h.

The proof is postponed to Section 4.1.

4 Inf-sup condition for the implicit error estimator

In this section we show that the computations using the implicit error estimation technique are stable in the sense that the local matrices in the bilinear form B_K in (3.3) remain uniformly well conditioned. Equivalently, we prove that they satisfy the inf-sup condition uniformly.

Theorem 4 *The bilinear form* $B_K : \mathcal{N}_2^2(K) \times \mathcal{N}_2^2(K) \to \mathbb{R}$ *satisfies the inf-sup condition uniformly in* K*; namely there is a positive constant* h_0 *such that for any non-degenerated family of tetrahedra* $\mathcal{T}_h$ *and for any element* $K \in \mathcal{T}_h$ *with diam* $K < h_0$ *and any* $\boldsymbol{u} \in \mathcal{N}_2^2(K)$

$$\sup_{\boldsymbol{v} \in \mathcal{N}_2^2(K)} \frac{|B_K(\boldsymbol{u},\boldsymbol{v})|}{\|\boldsymbol{v}\|_{\mathrm{curl},K}} \ge \min\{\frac{1}{2}, k^2\}\|\boldsymbol{u}\|_{\mathrm{curl},K}.$$

To prove this theorem we first give the explicit expression of the bilinear form B_K in terms of the original basis functions. Using (3.6) we obtain that for any $\boldsymbol{v} = \sum_{i=1}^8 v_i\boldsymbol{\phi}_i \in \mathcal{N}_2^2(K)$

$$\begin{aligned}(\boldsymbol{v},\boldsymbol{v})_K &= (\sum_{i=1}^8 v_i\boldsymbol{\phi}_i, \sum_{j=1}^8 v_j\boldsymbol{\phi}_j)_K \\ &= |\det \mathrm{d}D_K|((\mathrm{d}D_K^{-1})^T\sum_{i=1}^8 v_i\boldsymbol{\phi}_i^0, (\mathrm{d}D_K^{-1})^T\sum_{j=1}^8 v_j\boldsymbol{\phi}_j^0)_{\hat{K}}.\end{aligned} \tag{4.1}$$

Using (3.6) one can easily prove (see [27], Corollary 3.58) that

$$\mathrm{curl}_{x,y,z}\boldsymbol{\phi}_j = \frac{1}{\det \mathrm{d}D_K}\mathrm{d}D_K\mathrm{curl}_{\xi,\eta,\zeta}\boldsymbol{\phi}_j^0, \quad j = 1,2,\ldots,8. \tag{4.2}$$

Therefore,

$$(\operatorname{curl} \boldsymbol{v}, \operatorname{curl} \boldsymbol{v})_K = (\operatorname{curl}_{x,y,z} \sum_{i=1}^{8} v_i \boldsymbol{\phi}_i, \operatorname{curl}_{x,y,z} \sum_{j=1}^{8} v_j \boldsymbol{\phi}_j)_K \tag{4.3}$$
$$= \frac{1}{|\det \mathrm{d}D_K|} (\mathrm{d}D_K \operatorname{curl}_{\xi,\eta,\zeta} \sum_{i=1}^{8} v_i \boldsymbol{\phi}_i^0, \mathrm{d}D_K \operatorname{curl}_{\xi,\eta,\zeta} \sum_{j=1}^{8} v_j \boldsymbol{\phi}_j^0)_{\hat{K}}.$$

We also use the following two lemmas:

Lemma 5 *Let us denote with $\mathcal{T}_h^1$ a non-degenerated family of tetrahedra such that $\det \mathrm{d}D_K = 1$ for all $K \in \mathcal{T}_h^1$. Then there is a compact set $\mathcal{D} \subset \mathbb{R}^{3\times 3}$ such that $0 \notin \mathcal{D}$ and $\mathrm{d}D_K \in \mathcal{D}$ for all $K \in \mathcal{T}_h^1$.*

Proof We use the notion of the spectral norm which is given for an arbitrary matrix $D \in \mathbb{R}^{n\times n}$ as

$$\|D\|_{\mathrm{sp}} = \sup_{|\xi|=1} |D\xi|. \tag{4.4}$$

We can establish the lemma if we prove that there are positive constants C_1, C_2 such that for any $K \in \mathcal{T}_h^1$ the following inequality holds:

$$C_1 \le \|\mathrm{d}D_K\|_{\mathrm{sp}} \le C_2. \tag{4.5}$$

Then the set

$$\mathcal{D} = \overline{\{\mathrm{d}D_K : K \in \mathcal{T}_h^1\}}$$

is closed, and bounded with respect to the spectral norm (which is equivalent with any norm in $\mathbb{R}^{3\times 3}$), moreover, the condition $\det \mathrm{d}D_K = 1, \forall\ K \in \mathcal{T}_h^1$ implies that $0 \notin \mathcal{D}$.

Note that the condition $\det \mathrm{d}D_K = 1$ implies that the volume of any tetrahedron K is the same as that of $\hat{K}$.

By contradiction, assume first that there is no constant C_2 in (4.5), i.e. there is a sequence K_n such that $\|\mathrm{d}D_{K_n}\|_{\mathrm{sp}} > n$. Then according to Lemma 5.10 in [27]

$$n < \|\mathrm{d}D_{K_n}\|_{\mathrm{sp}} \le \frac{h_{K_n}}{\rho_{\hat{K}}},$$

where $h_{K_n} = \operatorname{diam} K_n$ and $\rho_{\hat{K}}$ denotes the radius of the largest ball contained in the reference element $\hat{K}$. Then $\lim_{n\to\infty} h_{K_n} = \infty$ while the condition on the volume implies that ρ_{K_n} remains bounded. This contradicts to the non-degeneracy property of the meshes.

Assume now that there is no positive lower bound C_1 in (4.5). Then according to (4.4) there is a sequence K_n such that

$$\max |\operatorname{eig} \mathrm{d}D_{K_n}| \le \|\mathrm{d}D_{K_n}\|_{\mathrm{sp}} = \sup_{|\xi|=1} |\mathrm{d}D_{K_n}\xi| < \frac{1}{n}, \tag{4.6}$$

where eig denotes an eigenvalue. Since the determinant is the product of the eigenvalues, this is again a contradiction. $\square$

Lemma 6 *For **any** $C > 0$ there is a positive number $h_0 \in \mathbb{R}^+$ such that for every non-degenerated family of tetrahedra $\mathcal{T}_h$ and for any element $K \in \mathcal{T}_h$ with $\operatorname{diam} K \le h_0$ and $\boldsymbol{u}_2 \in \mathcal{N}_2^2(K)$ with $\boldsymbol{u}_2 \perp \ker \operatorname{curl}$, the following inequality holds:*

$$(\operatorname{curl} \boldsymbol{u}_2, \operatorname{curl} \boldsymbol{u}_2)_K \ge C(\boldsymbol{u}_2, \boldsymbol{u}_2)_K. \tag{4.7}$$

Proof: First, we decompose the transformation D_K as follows: $D_K = D_K \tilde{D}_K^{-1} \circ \tilde{D}_K$, where

$$\tilde{D}_K = \frac{1}{\sqrt[3]{\det \mathrm{d}D_K}} D_K : \hat{K} \to \tilde{K} \tag{4.8}$$

and

$$D_K \tilde{D}_K^{-1} = \sqrt[3]{\det \mathrm{d}D_K} I : \tilde{K} \to K, \tag{4.9}$$

where the corresponding matrices are denoted with $\mathrm{d}D_K$, $\mathrm{d}\tilde{D}_K$ and $\mathrm{d}D_K \mathrm{d}\tilde{D}_K^{-1}$, respectively, and $\det \mathrm{d}\tilde{D}_K = 1$.
For a function $\boldsymbol{u}_2 = \sum_{i=1}^8 u_{2,i} \boldsymbol{\phi}_i \in \{\operatorname{span} \boldsymbol{\phi}_j\}_{j=1,\ldots,8}$ we define

$$\tilde{\boldsymbol{u}}_2 : \tilde{K} \to \mathbb{R}^3 \quad \text{with} \quad \tilde{\boldsymbol{u}}_2 = \sum_{i=1}^{8} u_{2,i} \tilde{\boldsymbol{\phi}}_i,$$

where the basis functions $\tilde{\boldsymbol{\phi}}_i : \tilde{K} \to \mathbb{R}^3$ $(i = 1, 2, \ldots, 8)$ are defined using (3.6) with the transformation $\tilde{D}_K$ instead of D_K. Using (4.1) for the linear mapping $D_K \tilde{D}_K^{-1}$ we obtain that

$$(\boldsymbol{u}_2, \boldsymbol{u}_2)_K = |\det \mathrm{d}D_K| \frac{1}{(\sqrt[3]{\det \mathrm{d}D_K})^2} (\tilde{\boldsymbol{u}}_2, \tilde{\boldsymbol{u}}_2)_{\tilde{K}} \tag{4.10}$$

and using (4.3) gives that

$$(\operatorname{curl} \boldsymbol{u}_2, \operatorname{curl} \boldsymbol{u}_2)_K = \frac{1}{|\det \mathrm{d}D_K|} (\sqrt[3]{\det \mathrm{d}D_K})^2 (\operatorname{curl} \tilde{\boldsymbol{u}}_2, \operatorname{curl} \tilde{\boldsymbol{u}}_2)_{\tilde{K}}. \tag{4.11}$$

Using then (4.1) and (4.3) and the transformation formula (3.6) we obtain that for $\boldsymbol{u}_2 = \sum_{i=1}^8 u_{2,i} \boldsymbol{\phi}_i \in \{\operatorname{span} \boldsymbol{\phi}_j\}_{j=1,\ldots,8} \cap \ker \operatorname{curl}^\perp$ (which can be identified with the coefficients $u_{2,i}$) and $\mathrm{d}\tilde{D}_K \in \mathbb{R}^{3\times3}$ the mapping of type $\mathbb{R}^8 \times \mathbb{R}^{3\times3} \to \mathbb{R}$ defined by

$$[\boldsymbol{u}_2, \mathrm{d}\tilde{D}_K] \to \frac{(\operatorname{curl} \tilde{\boldsymbol{u}}_2, \operatorname{curl} \tilde{\boldsymbol{u}}_2)_{\tilde{K}}}{(\tilde{\boldsymbol{u}}_2, \tilde{\boldsymbol{u}}_2)_{\tilde{K}}} \tag{4.12}$$

is a continuous function of type $\mathbb{R}^8 \times \mathbb{R}^{3\times3} \to \mathbb{R}^+$. We may assume that it is given only on the unit sphere of $\mathbb{R}^8$, since $\lambda \boldsymbol{u}_2$ and $\boldsymbol{u}_2$ result in the same values in (4.12). In this way, the mapping in (4.12) is given on a compact set, see Lemma 5. Therefore its infimum equals to its minimum, which should be positive. Using this with the relations in (4.10) and (4.11) we obtain that for any $\mathrm{d}D_K \in \mathbb{R}^{3\times 3}$ and $(u_{2,1}, u_{2,2}, \dots, u_{2,8}) \in \mathbb{R}^8$

$$0 < \tilde{c} \le \frac{(\operatorname{curl} \tilde{\boldsymbol{u}}_2, \operatorname{curl} \tilde{\boldsymbol{u}}_2)_{\tilde{K}}}{(\tilde{\boldsymbol{u}}_2, \tilde{\boldsymbol{u}}_2)_{\tilde{K}}} = (\sqrt[3]{\det \mathrm{d}D_K})^2 \frac{(\operatorname{curl} \boldsymbol{u}_2, \operatorname{curl} \boldsymbol{u}_2)_K}{(\boldsymbol{u}_2, \boldsymbol{u}_2)_K}. \tag{4.13}$$

Obviously, $(\operatorname{curl} \boldsymbol{u}_2, \operatorname{curl} \boldsymbol{u}_2)_K \ge \dfrac{\tilde{c}}{(\sqrt[3]{\det \mathrm{d}D_K})^2}(\boldsymbol{u}_2, \boldsymbol{u}_2)_K$, and $\det \mathrm{d}D_K \to 0$ as the diameter of K converges to zero, then for some h_0 we will have $\dfrac{\tilde{c}}{(\sqrt[3]{\det \mathrm{d}D_K})^2} \ge C$ in (4.7), which proves the lemma. $\square$

Proof of Theorem 4: Decompose $\boldsymbol{u} \in \mathcal{N}_2^2(K)$ as $\boldsymbol{u} = \boldsymbol{u}_1 + \boldsymbol{u}_2$, where $\operatorname{curl} \boldsymbol{u}_1 = 0$ and $\boldsymbol{u}_2 \perp \ker \operatorname{curl}$. Then, for a given $\boldsymbol{u}$ choose $\boldsymbol{v} = \boldsymbol{u}_1 - \boldsymbol{u}_2$ and with this

$$\begin{aligned} |B_K(\boldsymbol{u}, \boldsymbol{v})| &= |-(\operatorname{curl} \boldsymbol{u}_2, \operatorname{curl} \boldsymbol{u}_2)_K - k^2(\boldsymbol{u}_1 + \boldsymbol{u}_2, \boldsymbol{u}_1 - \boldsymbol{u}_2)_K| \\ &= |(\operatorname{curl} \boldsymbol{u}_2, \operatorname{curl} \boldsymbol{u}_2)_K - k^2(\boldsymbol{u}_2, \boldsymbol{u}_2)_K + k^2(\boldsymbol{u}_1, \boldsymbol{u}_1)_K|. \end{aligned} \tag{4.14}$$

On the other hand,

$$\begin{aligned} \|\boldsymbol{u}\|_{\mathrm{curl},K} \|\boldsymbol{v}\|_{\mathrm{curl},K} &= \|\boldsymbol{u}_1 + \boldsymbol{u}_2\|_{\mathrm{curl},K} \|\boldsymbol{u}_1 - \boldsymbol{u}_2\|_{\mathrm{curl},K} \\ &= (\|\boldsymbol{u}_1\|^2_{\mathrm{curl},K} + \|\boldsymbol{u}_2\|^2_{\mathrm{curl},K})^{\frac{1}{2}} (\|\boldsymbol{u}_1\|^2_{\mathrm{curl},K} + \|\boldsymbol{u}_2\|^2_{\mathrm{curl},K})^{\frac{1}{2}} \\ &= \|\boldsymbol{u}_1\|^2_{\mathrm{curl},K} + \|\boldsymbol{u}_2\|^2_{\mathrm{curl},K} \\ &= (\operatorname{curl} \boldsymbol{u}_2, \operatorname{curl} \boldsymbol{u}_2)_K + (\boldsymbol{u}_2, \boldsymbol{u}_2)_K + (\boldsymbol{u}_1, \boldsymbol{u}_1)_K. \end{aligned} \tag{4.15}$$

Using Lemma 6 with $C = 2k^2 + 1$ there is an $h_0 > 0$ such that for any K with $\operatorname{diam} K < h_0$

$$\begin{aligned} &(\operatorname{curl} \boldsymbol{u}_2, \operatorname{curl} \boldsymbol{u}_2)_K - k^2(\boldsymbol{u}_2, \boldsymbol{u}_2)_K \\ &\ge \frac{1}{2}(\operatorname{curl} \boldsymbol{u}_2, \operatorname{curl} \boldsymbol{u}_2)_K + (k^2 + \frac{1}{2})(\boldsymbol{u}_2, \boldsymbol{u}_2)_K - k^2(\boldsymbol{u}_2, \boldsymbol{u}_2)_K \\ &= \frac{1}{2}((\operatorname{curl} \boldsymbol{u}_2, \operatorname{curl} \boldsymbol{u}_2)_K + (\boldsymbol{u}_2, \boldsymbol{u}_2)_K). \end{aligned}$$

Inserting this into (4.14) and using (4.15) we obtain that for every K, with $\operatorname{diam} K < h_0$, that

$$\begin{aligned} |B_K(\boldsymbol{u}, \boldsymbol{v})| &\ge (\operatorname{curl} \boldsymbol{u}_2, \operatorname{curl} \boldsymbol{u}_2)_K - k^2(\boldsymbol{u}_2, \boldsymbol{u}_2)_K + k^2(\boldsymbol{u}_1, \boldsymbol{u}_1)_K \\ &\ge \min\{\frac{1}{2}, k^2\}((\operatorname{curl} \boldsymbol{u}_2, \operatorname{curl} \boldsymbol{u}_2)_K + (\boldsymbol{u}_2, \boldsymbol{u}_2)_K + (\boldsymbol{u}_1, \boldsymbol{u}_1)_K) \\ &= \min\{\frac{1}{2}, k^2\}\|\boldsymbol{u}\|_{\mathrm{curl},K} \|\boldsymbol{v}\|_{\mathrm{curl},K}. \end{aligned}$$

Summarized, there is a $h_0 > 0$ such that for any non-degenerate tetrahedron K with $\operatorname{diam} K < h_0$ and for an arbitrary $\boldsymbol{u} \in \mathcal{N}_2^2(K)$ one can find $\boldsymbol{v} \in \mathcal{N}_2^2(K)$ such that

$$|B_K(\boldsymbol{u}, \boldsymbol{v})| \ge \min\{\frac{1}{2}, k^2\}\|\boldsymbol{u}\|_{\mathrm{curl},K} \|\boldsymbol{v}\|_{\mathrm{curl},K}.$$

Dividing both sides with $\|\boldsymbol{v}\|_{\mathrm{curl},K}$ gives the statement of the theorem. $\square$

We can sharpen the result of Theorem 4 further and compute the dependence of the critical mesh size h_0 on the wavenumber k. Accordingly, we use the notation $B_{K,\alpha}$ for the bilinear form on $H(\text{curl}, K) \times H(\text{curl}, K)$ with

$$B_{K,\alpha}(\boldsymbol{u}, \boldsymbol{v}) = (\text{curl}\, \boldsymbol{u}, \text{curl}\, \boldsymbol{v})_K - (\alpha k)^2 (\boldsymbol{u}, \boldsymbol{v})_K,$$

where $\alpha > 1$ is a given parameter.

Lemma 7 *Assume that Theorem 4 holds for the wavenumber k with the constant h_0. Then for any $K \in \mathcal{T}_h$ with diam $K < \frac{1}{\alpha} h_0$, any $\alpha > 1$ and any $\boldsymbol{u} \in \mathcal{N}_2^2(K)$ we have for the wave number αk the inf-sup condition*

$$\sup_{\boldsymbol{v} \in \mathcal{N}_2^2(K)} \frac{|B_{K,\alpha}(\boldsymbol{u}, \boldsymbol{v})|}{\|\boldsymbol{v}\|_{\text{curl},K}} \geq \min\{\frac{1}{2}, k^2\} \|\boldsymbol{u}\|_{\text{curl},K} \tag{4.16}$$

Proof We use (4.1) and (4.3) in the case when $\tilde{K}$ is a tetrahedron with diam $\tilde{K} < h_0$ and $D_\alpha : \tilde{K} \to K$ is defined by $D_\alpha = \frac{1}{\alpha} I$.

$$\begin{aligned}
\sup_{\boldsymbol{v} \in \mathcal{N}_2^2(K)} \frac{|B_{K,\alpha}(\boldsymbol{u}, \boldsymbol{v})|}{\|\boldsymbol{v}\|_{\text{curl},K}} &= \sup_{\boldsymbol{v} \in \mathcal{N}_2^2(K)} \frac{|(\text{curl}\, \boldsymbol{u}, \text{curl}\, \boldsymbol{v})_K - (\alpha k)^2 (\boldsymbol{u}, \boldsymbol{v})_K|}{\|\boldsymbol{v}\|_{\text{curl},K}} \\
&= \sup_{\tilde{\boldsymbol{v}} \in \mathcal{N}_2^2(\tilde{K})} \frac{|\alpha (\text{curl}\, \tilde{\boldsymbol{u}}, \text{curl}\, \tilde{\boldsymbol{v}})_{\tilde{K}} - \frac{1}{\alpha} (\alpha k)^2 (\tilde{\boldsymbol{u}}, \tilde{\boldsymbol{v}})_{\tilde{K}}|}{\sqrt{\alpha (\text{curl}\, \tilde{\boldsymbol{v}}, \text{curl}\, \tilde{\boldsymbol{v}})_{\tilde{K}} + \frac{1}{\alpha} (\tilde{\boldsymbol{v}}, \tilde{\boldsymbol{v}})_{\tilde{K}}}} \\
&\geq \sqrt{\alpha} \sup_{\tilde{\boldsymbol{v}} \in \mathcal{N}_2^2(\tilde{K})} \frac{|(\text{curl}\, \tilde{\boldsymbol{u}}, \text{curl}\, \tilde{\boldsymbol{v}})_{\tilde{K}} - k^2 (\tilde{\boldsymbol{u}}, \tilde{\boldsymbol{v}})_{\tilde{K}}|}{\|\tilde{\boldsymbol{v}}\|_{\text{curl},\tilde{K}}} \\
&\geq \min\{\frac{1}{2}, k^2\} \sqrt{\alpha} \sqrt{\|\text{curl}\, \tilde{\boldsymbol{u}}\|^2_{[L_2(\tilde{K})]^3} + \|\tilde{\boldsymbol{u}}\|^2_{[L_2(\tilde{K})]^3}} \\
&= \min\{\frac{1}{2}, k^2\} \sqrt{\alpha} \sqrt{\frac{1}{\alpha} \|\text{curl}\, \boldsymbol{u}\|^2_{[L_2(K)]^3} + \alpha \|\boldsymbol{u}\|^2_{[L_2(K)]^3}} \\
&= \min\{\frac{1}{2}, k^2\} \sqrt{\|\text{curl}\, \boldsymbol{u}\|^2_{[L_2(K)]^3} + \alpha^2 \|\boldsymbol{u}\|^2_{[L_2(K)]^3}} \geq \min\{\frac{1}{2}, k^2\} \|\boldsymbol{u}\|_{\text{curl},K},
\end{aligned}$$

where (4.1) and (4.3) were applied in the second line, Theorem 4 in the fourth line and again (4.1) and (4.3) in the fifth line. $\square$

Remark 8 *Lemma 7 shows that for the inf-sup condition we only need that kh is smaller than some positive constant.*

Using Lemma 7 and some results in [25] we can prove the k-dependence of the constant C on the right hand side of (3.9).

Proof of Theorem 3: According to Theorem 3 in [25]

$$\|\hat{\boldsymbol{e}}_h\|^2_{\text{curl},K} \leq C_1^2 C_2((1+k^2)^2\|\hat{\boldsymbol{e}}_h\|^2_{\text{curl},K} + h^2\|\bar{\boldsymbol{r}} - \boldsymbol{r}\|^2_{[L_2(K)]^3} + h\|\bar{\boldsymbol{R}} - \boldsymbol{R}\|^2_{[L_2(K)]^3}),$$

where C_2 does not depend on h and k, and $C_1 = \frac{1}{\min\{\frac{1}{2},k^2\}}$ is the inverse of the constant in the inf-sup condition. For wave numbers $k \geq \sqrt{\frac{1}{2}}$ we obtain $C_1^2 = 4$.

The proof was carried out for rectangular elements in [25] but it is applicable also for tetrahedral elements if Section 4.1 in [25] is changed accordingly. This requires a standard bubble function technique which only uses the non-degenerate property of the mesh. We omit this straightforward but lengthy analysis. □

5 Adaptive mesh generation

In this section we describe how to use the implicit a posteriori error estimation technique in real applications. Let us define the exact error δ_K, which is unknown in practice, and the implicit *local error estimate* (*indicator*) $\hat{\delta}_K$ on element K by

$$\delta_K = \|\boldsymbol{E} - \boldsymbol{E}_h\|_{\text{curl},K}, \quad \hat{\delta}_K = \|\hat{\boldsymbol{e}}_h\|_{\text{curl},K}. \tag{5.1}$$

Recall that $\boldsymbol{E}_h$ denotes the numerical solution of the Maxwell equations (2.1) obtained by using the first order edge finite elements (see Section 2.1) and that $\hat{\boldsymbol{e}}_h$ denotes the computed error with the implicit error estimator, defined in (3.7), and solved with the help of the finite element space $\mathcal{N}_2^2(K)$ (see Section 3.2.2).

The exact global error δ and the implicit global error estimate δ_h can be obtained as

$$\delta = \left(\sum_{K\in\mathcal{T}_h} \delta_K^2\right)^{1/2}, \quad \delta_h = \left(\sum_{K\in\mathcal{T}_h} \hat{\delta}_K^2\right)^{1/2}. \tag{5.2}$$

Accordingly, if we sum up the terms in (3.9), we obtain

$$\delta_h \leq C(1+k^2)\delta,$$

where C does not depend on h and k.

For a given tolerance `TOL` we aim to construct a mesh $\mathcal{T}_h$ such that

$$\delta_h < \texttt{TOL}. \tag{5.3}$$

There are several adaptation strategies to achieve this.

Strategy 1. In this strategy, proposed in [21], the algorithm tries to equidistribute the local error over all elements of $\mathcal{T}_h$. Thus, we insist that for all elements K in the tessellation $\mathcal{T}_h$ the condition $\hat{\delta}_K \approx \frac{\mathtt{TOL}}{\sqrt{N}}$ is satisfied, where N denotes the total number of elements in the tessellation. Element K in the mesh $\mathcal{T}_h$ is marked for refinement if

$$\hat{\delta}_K > \frac{\mathtt{TOL}}{\sqrt{N}}.$$

Strategy 2. This algorithm is based on an area-weighted tolerance approach. For given element K denote by V_K its volume. Then element K is marked for refinement if

$$\hat{\delta}_K > \mathtt{TOL}\sqrt{\frac{V_K}{V_\Omega}},$$

where V_Ω is the volume of the domain Ω. This strategy coincides with Strategy 1 if all elements in the tessellation have the same volume.

Strategy 3. An alternative strategy for error balancing is to refine the element K where the computed error estimate $\hat{\delta}_K$ exceeds a certain fraction of the total (or maximum) estimated error [21].

Strategy 4. One can also choose to refine a given percentage of the elements whose error indicator is the largest.

In [39] the authors study several adaptation strategies, such as fixed threshold, error equidistribution and error density equidistribution strategies, but the fixed fraction Strategy 4 appears to be the most useful, because in their experiments the other strategies can lead to an unacceptable decrease in the error reduction rate or even to a stagnation or oscillatory behavior in the error reduction.

It is also argued in [21] that Strategy 4 is preferable compared to the other algorithms. Therefore in the rest of this article mesh adaptation Strategy 4 is used in all numerical experiments.

Remark 9 (Computational costs) *In the adaptation algorithm we allow a growth in the number of degrees of freedom with a factor of at most* 3.5*, see* (6.3)*. It is realistic to assume that the computational work for these problems when using minimum residual (MINRES) iterative solver [37,42] is proportional to the squared number of degrees of freedom. Then the solution of the linear system on the adapted mesh with the MINRES iterative solver will require at most* $3.5^2 = 12.25$ *times more operation than on the original mesh. During the global mesh refinement each tetrahedron is subdivided into 8 elements and the resulting matrices are approximately* 8^2 *times larger than on the original mesh. Therefore, the solution of the linear system on the globally* *refined mesh will require at most* 64 *times more operation than on the original mesh. It is realistic to assume that the work required for the element-wise computation of the implicit error estimate is negligible and we obtain that the computational work on the globally refined mesh requires approximately* $\frac{64}{12.25} \approx 5.2$ *times more work than for the adaptive finite element solution. The computational work in terms of CPU time is presented in Section 6.1.2 and Figure 10.*

6 Numerical results

In this section we demonstrate the performance of the implicit error estimator (3.3) applied to the time harmonic Maxwell equations on a domain $\Omega \subset \mathbb{R}^3$. We choose the wavenumbers such that we can get rid of the major part of the pollution error [4]. Moreover, we expect that Theorem 3 provides an accurate lower estimate of the error. At the same time, on a fixed mesh, the implicit error estimate will become less effective when increasing the wave number due to the pollution error and lack of resolution to represent the wave on the finite element mesh.

The linear systems of discrete weak formulation (2.6) are solved using MINRES with diagonal preconditioner.

A good a posteriori error estimator should possess the following properties:

- The error estimator should be able to find those areas in the domain where the finite element solution has a large error.
- The error estimator should have a magnitude close to the real error, both locally and globally.

We verify the performance of the implicit error estimator for the Maxwell equations on five different test cases and define the effectivity index as

$$\varepsilon_h = \frac{\delta_h}{\delta}. \tag{6.1}$$

This quantity merely reflects the quality of the global error estimate but is useful to get an impression on the performance of the adaptive algorithm. For any adaptive algorithm the local behavior of the error is, however, one of the most important factors, therefore we evaluate the quality of the local error estimation by computing the correlation coefficient between $\{\delta_i\}_{i=1}^N$ and $\{\hat{\delta}_i\}_{i=1}^N$, where $\delta_i \equiv \delta_{K_i}$ and $\hat{\delta}_i \equiv \hat{\delta}_{K_i}$ are defined in (5.1).

Whenever the exact error δ_K is available we compute the correlation coefficient

[44] between the exact and estimated error as

$$r = \frac{N\sum_{j=1}^{N}\delta_j\hat{\delta}_j - \left(\sum_{j=1}^{N}\delta_j\right)\left(\sum_{j=1}^{N}\hat{\delta}_j\right)}{\sqrt{\left(N\sum_{j=1}^{N}\delta_j^2 - (\sum_{j=1}^{N}\delta_j)^2\right)\left(N\sum_{j=1}^{N}\hat{\delta}_j^2 - (\sum_{j=1}^{N}\hat{\delta}_j)^2\right)}}. \tag{6.2}$$

There is a strong correlation between $\{\delta_i\}_{i=1}^N$ and $\{\hat{\delta}_i\}_{i=1}^N$ if $r \geq 0.7$

In the experiments described in this section, the initial mesh is denoted by $\texttt{mesh}_0$, and the subsequent adapted meshes are denoted by $\texttt{mesh}_i$, $i = 1, 2, \ldots$. For adaptation we use the Centaur mesh generator [16] with the so called source based mesh generation technique. In this method regions where the mesh generator should create finer elements are called sources, which in our case are taken as spheres.

We organize the mesh adaptation as follows:

(1) Initialize $i = 0$ and N_{smax}.
(2) Solve problem (2.1) on $\texttt{mesh}_i$ and compute the implicit error estimate. Stop if the error satisfies (5.3).
(3) If the local error is almost homogeneously distributed over the elements then stop the adaptation procedure and apply global refinement. Set $i = i + 1$ and move to (2). Otherwise
(4) Mark $q\%$ of the elements with the largest error in the current mesh $\texttt{mesh}_i$ for adaptation. Based on these marked elements generate at most N_{smax} sources.
(5) Based on the created sources generate a new mesh and $i = i + 1$, then move to (2).

Based on the created source information, a new mesh is generated by Centaur such that

$$1.5 \leq \frac{N_{i+1}^{\mathrm{dof}}}{N_i^{\mathrm{dof}}} \leq 3.5, \tag{6.3}$$

where N_i^{dof} is the number of degrees of freedom (DOF) in $\texttt{mesh}_i$. Algorithm 1 describes the mesh adaptation procedure in detail.

The value of q can vary between $1\% - 20\%$ and is highly dependent on the mesh generation algorithm. In all our numerical experiments we have chosen $q = 1$ and $N_{\mathrm{smax}} = 15$. The small value of q is explained by the fact that the mesh generator Centaur creates meshes of high quality (no hanging nodes, no large dihedral angles in an element). A larger value of q would result therefore in a huge increase in the number of elements compared to the previous mesh which would not satisfy condition (6.3).

For the adaptation procedure it is also useful to have a lower bound for the exact error. In [25] a lower bound for the exact error is provided in terms of the implicit error estimate. This lower bound ensures that the resulting error estimate is not a pessimistic overestimate of the exact error when the mesh size is reduced.

Algorithm 1. Algorithm to create sources for adaptive mesh generation.

1: $N_{\text{smax}} = 15$ and $N_s = 0$
2: Reorder the elements according to their corresponding error in descending order. $N_m = [\frac{N}{100}]q$ - number of marked elements, N - number of elements in the mesh.
3: **for** $i = 1, \ldots, N_m$ **do**
4:   **if** $N_s = 0$ **then**
5:     create a source with a center located in the barycenter of element i with radius $r = \max(r_s, r_i)$, where $r_s = \alpha \cdot L$ with L being the domain size and r_i the radius of the circumsphere of element i. The parameter α depends on the mesh generator and in all our numerical experiments we choose $\alpha = 0.08$.
6:     $N_s = 1$
7:   **else**
8:     **for** $j = 1, \ldots, N_s$ **do**
9:       **if** the barycenter of element i is inside source N_j **then**
10:         do nothing, exit loop 8, go to loop 3
11:       **else**
12:         create a new source as described in step 5
13:         $N_s = N_s + 1$
14:       **end if**
15:       **if** $N_s = N_{\text{smax}}$ **then**
16:         STOP the algorithm
17:       **end if**
18:     **end for**
19:   **end if**
20: **end for**

6.1 Cylindrical domain

In this subsection we test the adaptation method by solving the Maxwell equations on a section of a cylindrical domain shown in Figure 2 and defined as:

$$\Omega = \{(x, y, z) = (r\cos\phi, r\sin\phi, z) \in \mathbb{R}^3 : 0 < r < 1,\ 0 < \phi < 3\pi/2,\ 0 < z < 1\},$$

with the wave number $k = 1$.

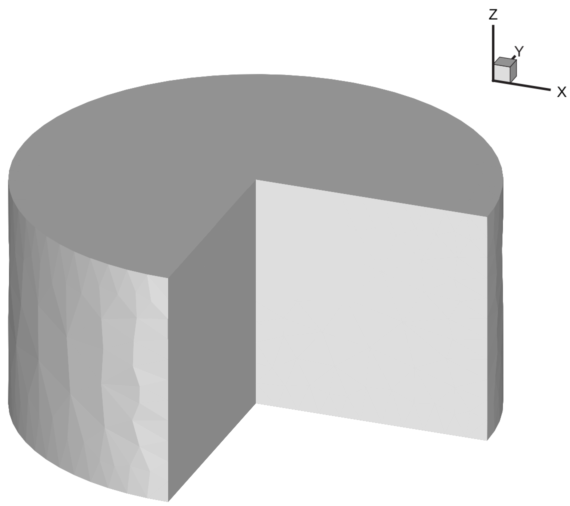

Fig. 2. Section of the cylindrical domain.

The solution of this problem has corner and edge singularities and can serve as a suitable test case. The adaptation algorithm should be able to detect this singular behavior and result in a denser mesh around the singularities.

6.1.1 Cylindrical domain with perfectly conducting boundary conditions

In order to be able to evaluate the true discretization errors we first choose a test problem with a known analytical solution. We pick up a vector field $\boldsymbol{E} = [E_1, E_2, E_3]$, substitute it into the first equation of (2.1) and obtain the corresponding right hand side function $\boldsymbol{J}$ and boundary conditions.

This test case is described in [30]. The exact solution of (2.1) is taken as

$$\boldsymbol{E} = z(1-z)(1-r^2)\nabla w, \quad \text{where} \quad w = r^{\frac{2}{3}} \sin(\frac{2}{3}\phi). \tag{6.4}$$

More specifically

$$\begin{aligned}
E_1 &= \frac{2}{3} z(1-z)(1-x^2-y^2) \frac{\sin(\frac{2}{3}\arctan\frac{y}{x})x - \cos(\frac{2}{3}\arctan\frac{y}{x})y}{(x^2+y^2)^{\frac{2}{3}}}, \\
E_2 &= \frac{2}{3} z(1-z)(1-x^2-y^2) \frac{\sin(\frac{2}{3}\arctan\frac{y}{x})y + \cos(\frac{2}{3}\arctan\frac{y}{x})x}{(x^2+y^2)^{\frac{2}{3}}}, \\
E_3 &= 0.
\end{aligned}$$

This function $\boldsymbol{E}$ has a typical singular behavior along the z axis and does not belong to $[H^1(\Omega)]^3$. For a discussion of its regularity see [30].

Table 2
Implicit error estimate δ_h, analytic error δ, effectivity index ε_h and correlation coefficient r on the cylindrical domain with perfectly conducting boundary conditions, see Section 6.1.1.

	# edges	# elements	δ_h	δ	ε_h	r
$\texttt{mesh}_0$	1231	981	0.3503	0.2038	1.71	0.57
$\texttt{mesh}_1$	2828	2259	0.1758	0.1268	1.38	0.80
$\texttt{mesh}_2$	10541	8607	0.1090	0.0787	1.38	0.78
$\texttt{mesh}_3$	17700	14550	0.0991	0.0708	1.39	0.80
$\texttt{mesh}_4$	44247	36826	0.0695	0.0518	1.34	0.80

For comparison purposes we also show the convergence of the error on globally refined meshes where the error is computed both using the implicit error estimator and the analytic expression. The lines corresponding to the locally and globally refined meshes are labelled with a subscript loc and glob, respectively. The numerical results and convergence plots are given in Table 2 and Figure 3. It is clear from Figure 3 that adapted meshes, constructed by the implicit error estimator, result in a smaller error than the globally refined meshes with the same number of degrees of freedom. It is also important to note that as the refinement procedure is continued the effectivity index remains constant $\varepsilon \approx 1.3$ and is close to one, which indicates that the error obtained from the implicit error estimator is a good approximation of the true error. The correlation coefficients in Table 2 indicate strong correlation, which means that the local error distribution predicted by the implicit a posteriori error estimation method is very similar to the exact error distribution, see Figure 4. On the left hand side of Figure 5 a contour plot of the implicit error estimate on the fourth adapted mesh is given. The elements with larger error are mainly concentrated near the singularity line along the z axis. The right hand side plot shows the corresponding adapted mesh where, as we expected, the finer elements are created along the singularity axis z.

6.1.2 Cylindrical domain with non-homogeneous tangential boundary conditions

In (6.4), the factor $z(1-z)(1-r^2)$ in front of ∇w was used to satisfy the perfectly conducting boundary conditions and appears to play a regularizing role. In the following test case we solve the Maxwell equations with a non-homogeneous tangential condition on the boundary of Ω, where the same domain is used as in the previous example, with the exact solution of the form

$$E = z\nabla w, \tag{6.5}$$

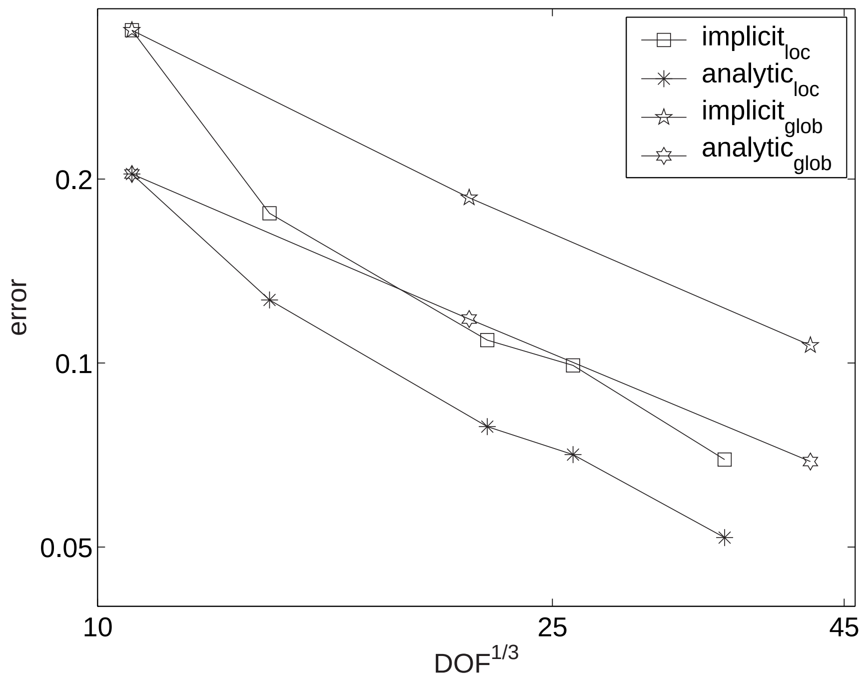

Fig. 3. Convergence plot in *loglog* scale for the cylindrical domain test case with perfectly conducting boundary conditions, see Section 6.1.1.

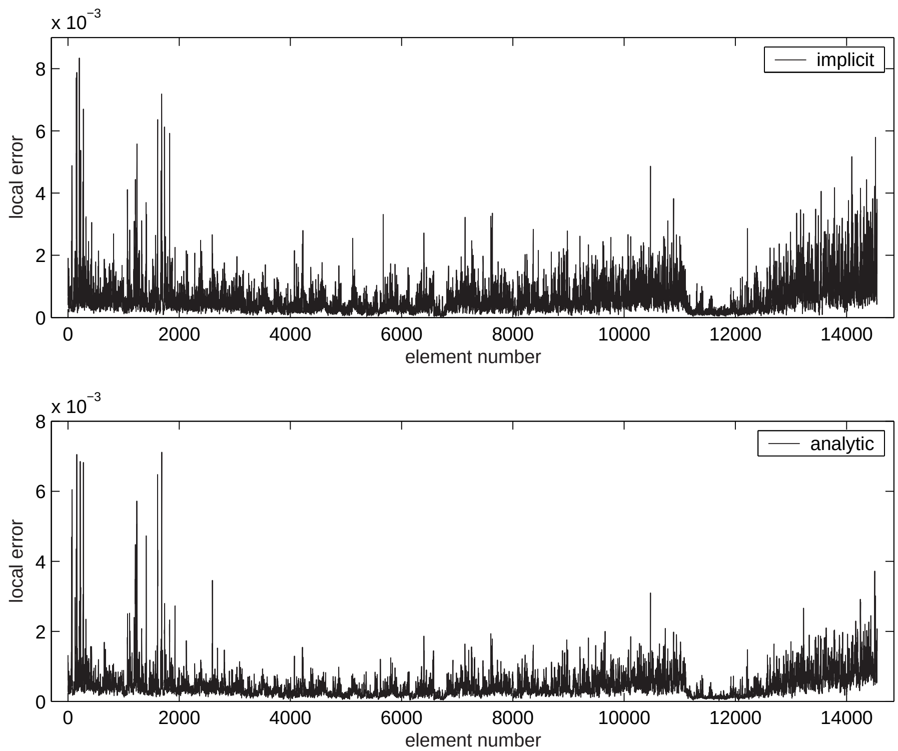

Fig. 4. Element-wise error distribution of the implicit error estimate and the exact error on the fourth adapted mesh in the cylindrical domain with perfectly conducting boundary conditions, see Section 6.1.1.

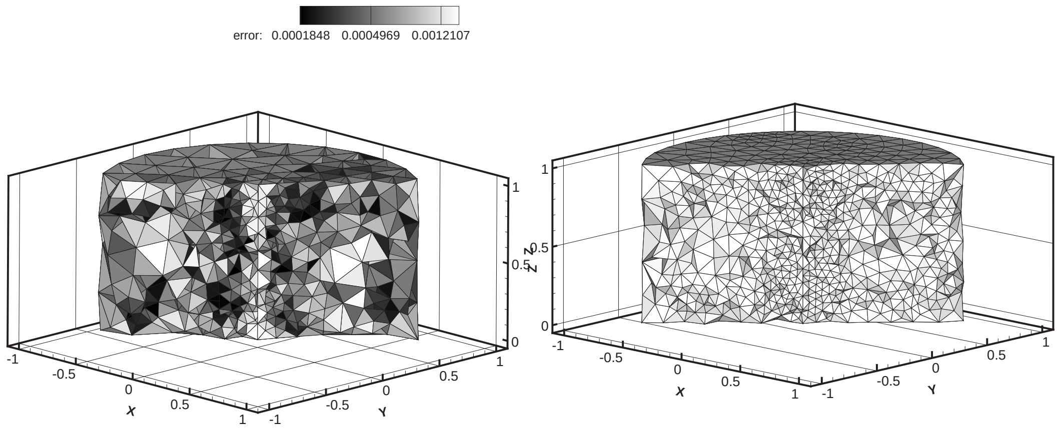

Fig. 5. Distribution of the implicit error estimate on the fourth adapted mesh (left) and the resulting adapted finite element mesh (right) in the cylindrical domain (cross section with $x = y$) using perfectly conducting boundary conditions, see Section 6.1.1

Table 3
Implicit error estimate δ_h, analytic error δ, effectivity index ε_h and correlation coefficient r on the cylindrical domain with non-homogeneous tangential boundary conditions, see Section 6.1.2.

	# edges	# elements	δ_h	δ	ε_h	r
$\mathtt{mesh}_0$	1231	981	0.2081	0.2209	0.91	0.68
$\mathtt{mesh}_1$	5219	4287	0.1286	0.1449	0.87	0.72
$\mathtt{mesh}_2$	10967	9018	0.0960	0.1156	0.83	0.78
$\mathtt{mesh}_3$	15277	12542	0.0922	0.1068	0.86	0.79
$\mathtt{mesh}_4$	26861	24853	0.0784	0.0936	0.83	0.80

with w defined in (6.4). This function, as well as its curl, have the same regularity as in the previous example [30].

The numerical results are given in Table 3 and the corresponding convergence diagrams are shown in Figure 6. The sequence of meshes used in this experiment are shown in Figure 8. We observe the same type of convergence for the implicit error estimator and the exact error as in the previous test case 6.1.1. We note that as the refinement procedure is continued the effectivity index remains constant $\varepsilon \approx 0.8$, which confirms the robustness of the method. The correlation coefficient is also within the range of strong correlation, which indicates a good prediction of the local error behavior. The local error distribution diagram on the final mesh (see Figure 9) is given in Figure 7. It clearly shows that the local error distribution of both schemes has the same behavior throughout the mesh. In Figure 9 a contour plot of the implicit error estimate

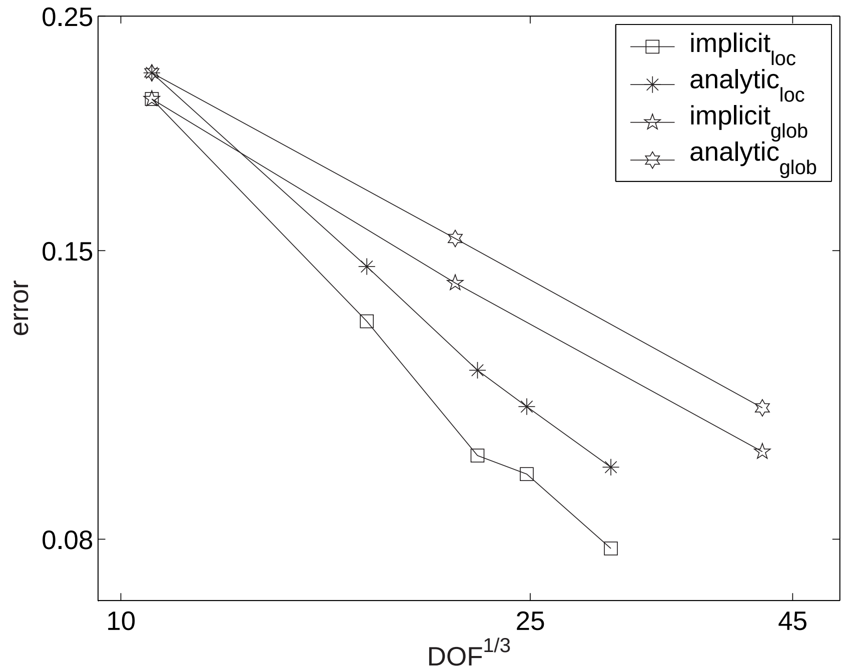

Fig. 6. Convergence plot in *loglog* scale for the cylindrical domain test case with non-homogeneous tangential boundary conditions, see Section 6.1.2.

on the final mesh is given. As expected, the elements with larger error are concentrated along the z axis.

To verify the work estimates discussed in Remark 9 we plot in Figure 10 the exact global error δ versus the CPU time, both on globally and adaptively refined meshes. It clearly shows that the adaptive algorithm is computationally more efficient than using globally refined meshes.

6.2 Fichera cube

The next test problem we consider are the Maxwell equations defined on a Fichera cube $\Omega = (-1,1)^3 \setminus [-1,0]^3$, with the wave number $k = 1$.

6.2.1 Fichera corner with non-homogeneous tangential boundary conditions

In this test $\boldsymbol{E} = \mathrm{grad}(r^{2/3}\sin(\frac{2}{3}t))$, with $r = \sqrt{x^2+y^2+z^2}$, $t = \arccos(\frac{xyz}{r})$.

More specifically

$$E_1 = -\frac{2}{3}\frac{(z^3y + zy^3)\cos(\frac{2}{3}\arccos(\frac{xyz}{\sqrt{x^2+y^2+z^2}}))}{\sqrt{x^2+y^2+z^2-x^2y^2z^2}(x^2+y^2+z^2)^{4/3}} + \frac{2}{3}\frac{\sin(\frac{2}{3}\arccos(\frac{xyz}{\sqrt{x^2+y^2+z^2}}))x}{(x^2+y^2+z^2)^{2/3}},$$

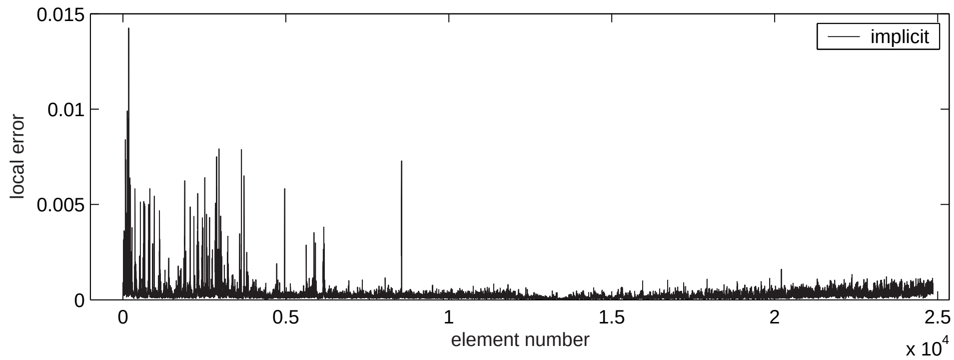

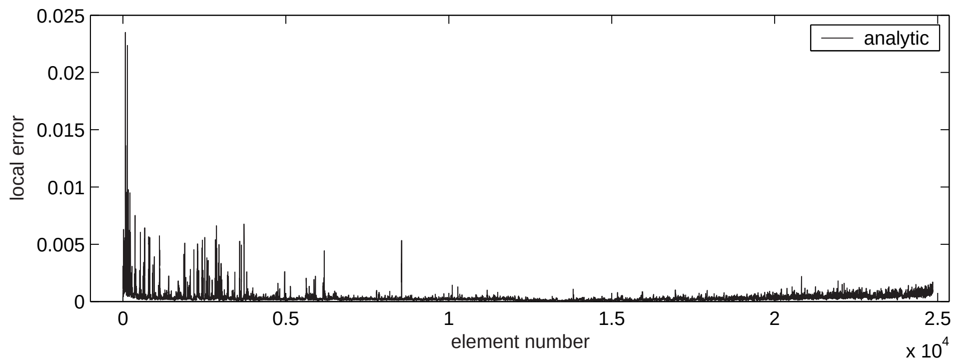

Fig. 7. Element-wise error distribution of the implicit error estimate and the exact error on the fifth adapted mesh in the cylindrical domain with non-homogeneous tangential boundary conditions, see Section 6.1.2.

$$E_2 = -\frac{2}{3}\frac{(zx^3 + xz^3)\cos(\frac{2}{3}\arccos(\frac{xyz}{\sqrt{x^2+y^2+z^2}}))}{\sqrt{x^2+y^2+z^2-x^2y^2z^2}(x^2+y^2+z^2)^{4/3}} + \frac{2}{3}\frac{\sin(\frac{2}{3}\arccos(\frac{xyz}{\sqrt{x^2+y^2+z^2}}))y}{(x^2+y^2+z^2)^{2/3}},$$

$$E_3 = -\frac{2}{3}\frac{(yx^3 + xy^3)\cos(\frac{2}{3}\arccos(\frac{xyz}{\sqrt{x^2+y^2+z^2}}))}{\sqrt{x^2+y^2+z^2-x^2y^2z^2}(x^2+y^2+z^2)^{4/3}} + \frac{2}{3}\frac{\sin(\frac{2}{3}\arccos(\frac{xyz}{\sqrt{x^2+y^2+z^2}}))z}{(x^2+y^2+z^2)^{2/3}}.$$

This vector field has a singular behavior near the origin and it is clear that $\boldsymbol{E}$ does not belong to $[H^1(\Omega)]^3$.

In Table 4 the numerical results are given and the corresponding convergence plots of the errors are shown in Figure 11. We observe that the error in the adaptive algorithm requires a smaller number of degrees of freedom, when the implicit error estimation method is used to control the adaptation process, than for the globally refined meshes. During the mesh adaptation procedure the effectivity index is small, but remains roughly constant, which means that the error behavior of the implicit error estimation technique is similar to that of the analytic error except for a scaling factor. The correlation coefficients again indicate a strong correlation which means that the local error behavior of the implicit a posteriori error estimation method is very similar to the

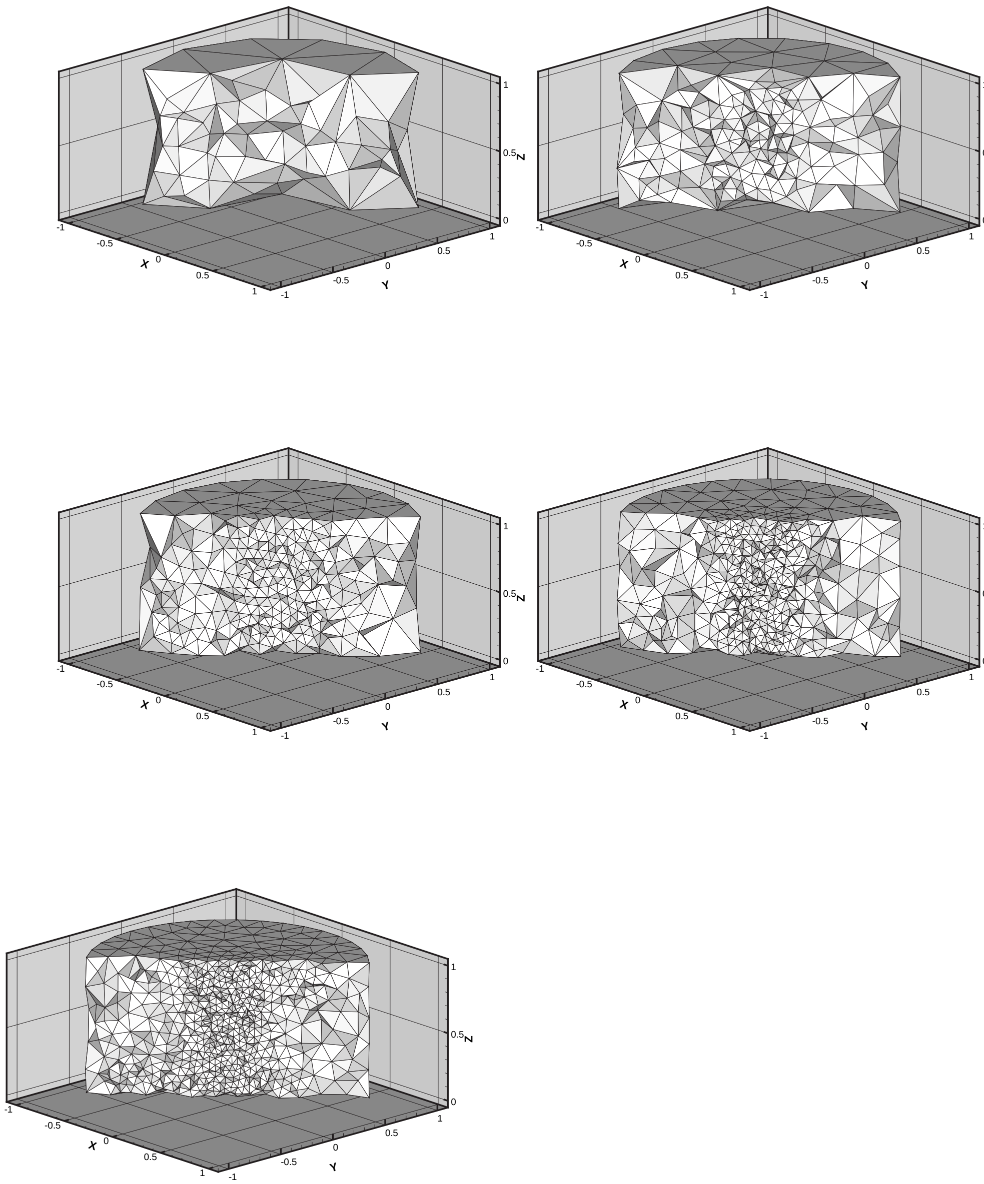

Fig. 8. Sequence of tetrahedral meshes based on the implicit error estimator used on the cylindrical domain with non-homogeneous tangential boundary conditions, see Section 6.1.2. Cross section with $x = y$.

exact error and is suitable to control the mesh adaptation. In Figure 12 a plot of the local error on the third adapted mesh, both for the implicit error estimate and the exact error, versus the element number is given. It also shows a clear correspondence between the local error predicted by the implicit a posteriori error estimation technique and the exact error. In the left hand side of Figure 13 a contour plot of the implicit error estimate on the third adapted

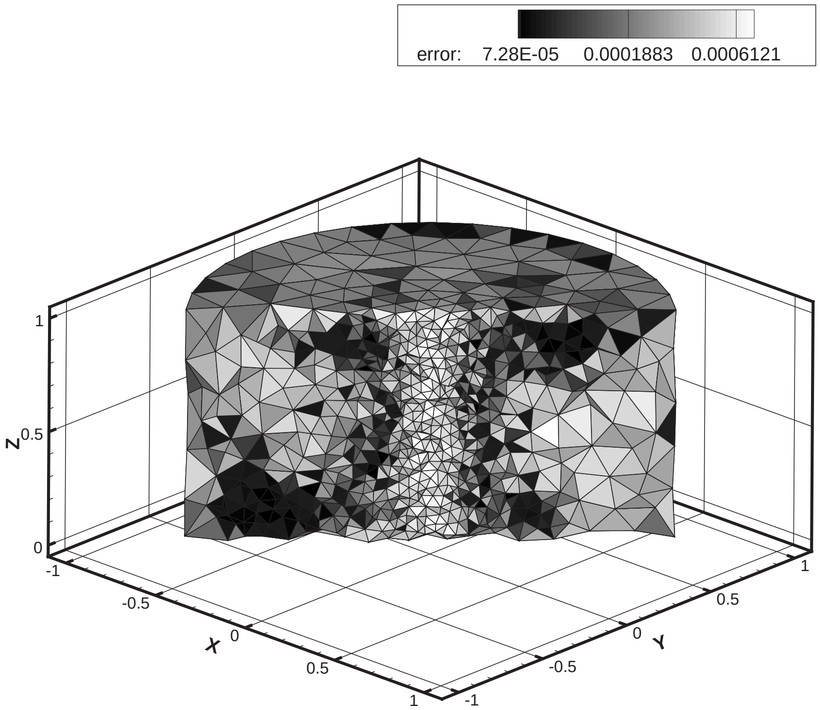

Fig. 9. Distribution of the implicit error estimate on the fifth adapted mesh used on the cylindrical domain with non-homogeneous tangential boundary conditions, see Section 6.1.2. Cross section with $x = y$.

mesh is given. The elements with a larger error are mostly concentrated near the Fichera corner. The right hand side plot shows the corresponding adapted mesh where, as we expected, the smaller elements are located near the Fichera corner and its neighborhood.

Note: The fact that the implicit error estimation technique predicts a significantly smaller error in this test case than the exact error can be explained by the fact that the exact solution is curl free. In this case when the curl of the numerical solution is "nearly" zero, the lower bound for the exact error provided by Theorem 3 in [25] reduces to a pessimistic estimate for the true error.

6.2.2 Fichera corner with perfectly conducting boundary conditions

In this test problem we consider the Maxwell equations on the same Fichera cube but now with perfectly conducting boundary conditions and a given right

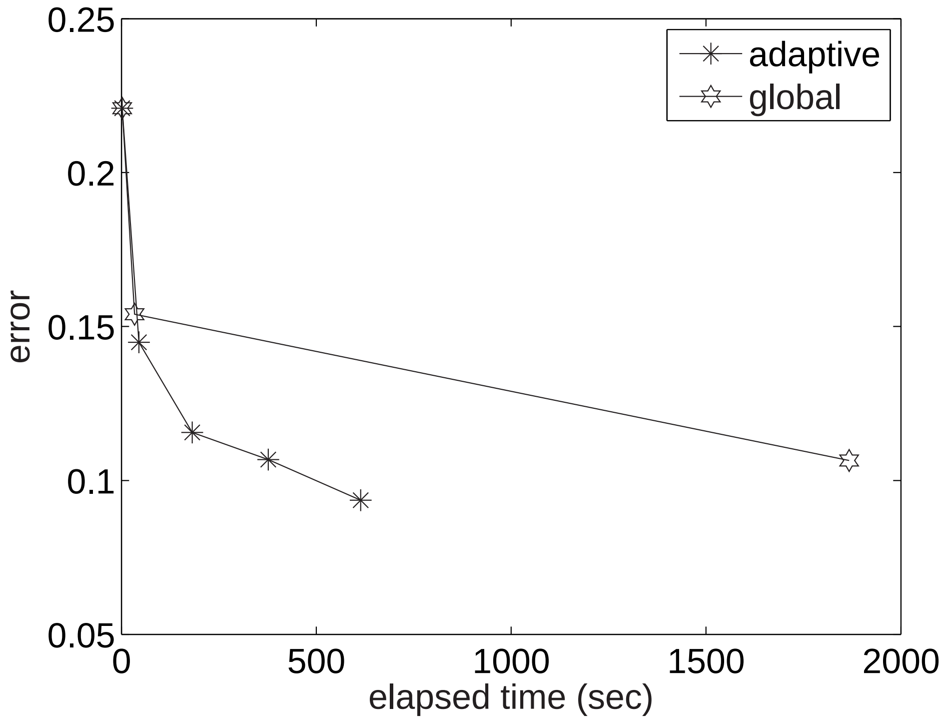

Fig. 10. Error versus CPU time on the cylindrical domain with non-homogeneous tangential boundary conditions, see Section 6.1.2.

Table 4
Implicit error estimate δ_h, analytic error δ, effectivity index ε_h and correlation coefficient r on the Fichera cube with non-homogeneous tangential boundary conditions, see Section 6.2.1.

	# edges	# elements	δ_h	δ	ε_h	r
$\texttt{mesh}_0$	930	710	0.1115	0.5558	0.20	0.70
$\texttt{mesh}_1$	3377	2716	0.0665	0.3972	0.16	0.82
$\texttt{mesh}_2$	9285	7588	0.0238	0.2436	0.096	0.74
$\texttt{mesh}_3$	14923	12293	0.0124	0.1880	0.066	0.80
$\texttt{mesh}_4$	30816	25642	0.0098	0.1485	0.066	0.72

hand side function

$$\boldsymbol{J} = \frac{1}{d^2} e^{-\frac{(x-\alpha)^2+(y-\alpha)^2+(z-\alpha)^2}{d^2}} \begin{pmatrix} \cos(\pi(y-\alpha))\cos(\pi(z-\alpha)) \\ \cos(\pi(z-\alpha))\cos(\pi(x-\alpha)) \\ \cos(\pi(x-\alpha))\cos(\pi(y-\alpha)) \end{pmatrix},$$

where $d = 0.5$, $\alpha = 0.25$.

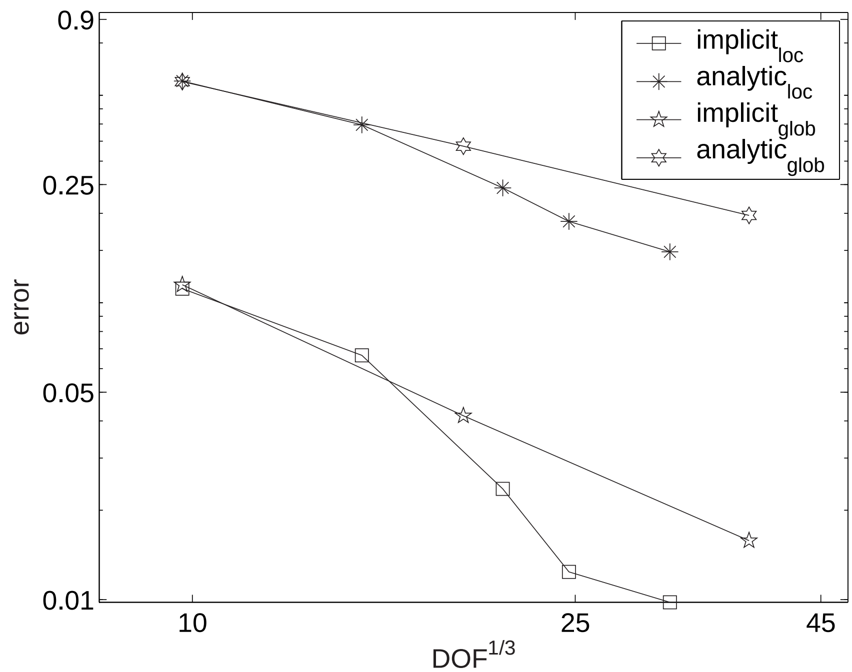

Fig. 11. Convergence plot in *loglog* scale for the Fichera cube test case with non-homogeneous tangential boundary conditions, see Section 6.2.1.

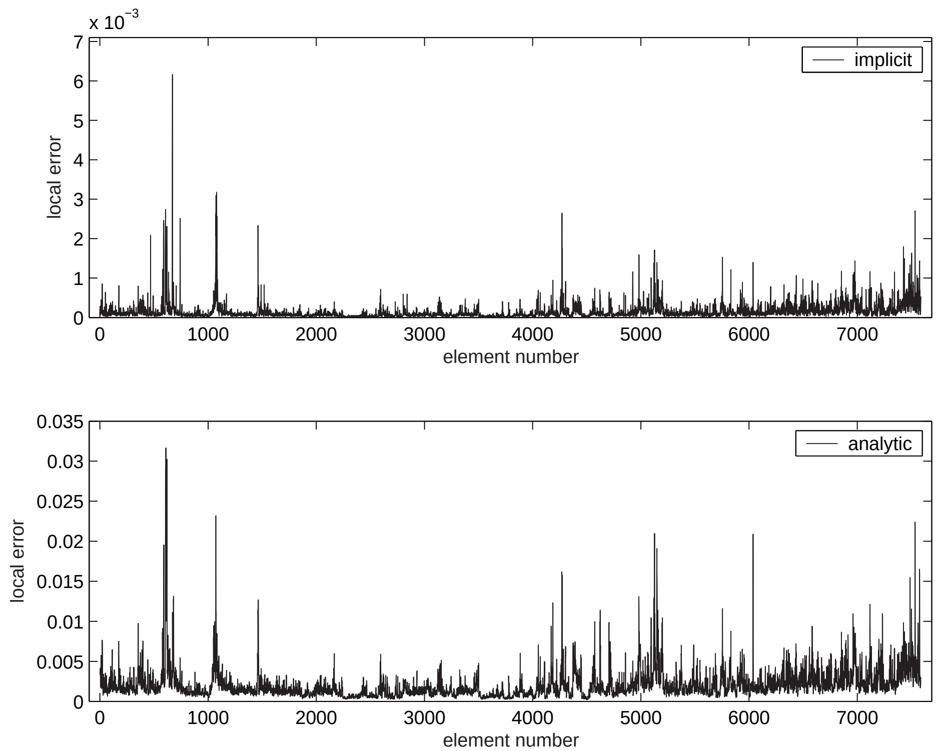

Fig. 12. Element-wise error distribution of the implicit error estimate and the exact error on the third adapted mesh used for the Fichera domain with non-homogeneous tangential boundary conditions, see Section 6.2.1.

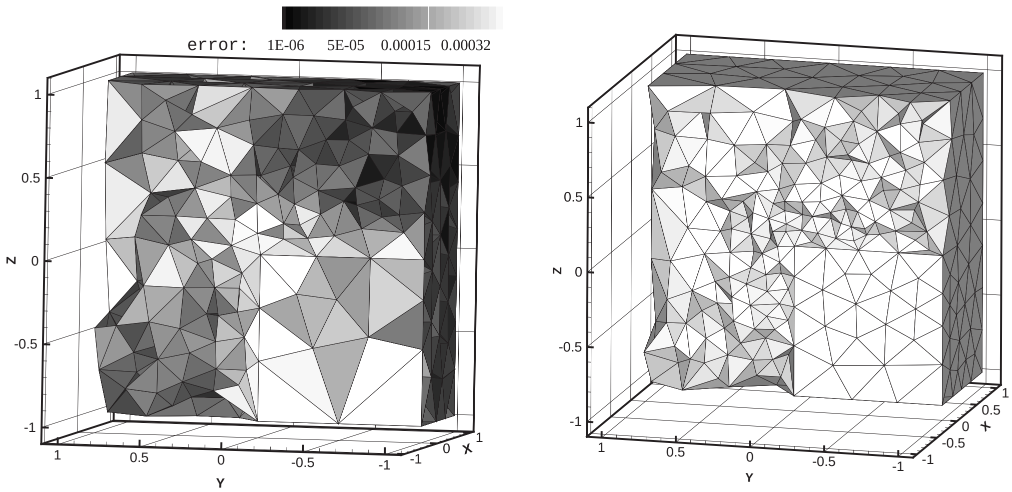

Fig. 13. Distribution of the implicit error estimate on the third adapted mesh (left) and the adapted finite element mesh of the fourth adapted mesh (right) used on the Fichera domain with non-homogeneous tangential boundary conditions, see Section 6.2.1. Cross section with $y = 0$.

Table 5
Implicit error estimate δ_h on the Fichera cube with perfectly conducting boundary conditions, see Section 6.2.2.

	# edges	# elements	δ_h
$\mathtt{mesh}_0$	898	683	0.3586
$\mathtt{mesh}_1$	2874	2247	0.2410
$\mathtt{mesh}_2$	8574	6939	0.1584
$\mathtt{mesh}_3$	29689	24497	0.1302
$\mathtt{mesh}_4$	62575	51969	0.0943

For this problem the exact analytic solution is unknown, therefore the numerical results are presented only for the implicit error estimator, see Table 5 and Figure 14.

It is clear that the adapted scheme using the implicit error estimation technique produces a smaller error for the same number of degrees of freedom as compared to the error obtained on the globally refined meshes. The rate of convergence of the implicit error estimator is also higher than that on the globally refined meshes.

The large correlation coefficients observed in all our numerical experiments (of course, except the last case, where it is not available) indicate that the error distribution predicted by the implicit error estimator is very similar to the error distribution of the exact error. This important property is obtained thanks to the choice of the local basis used for the finite element solution of

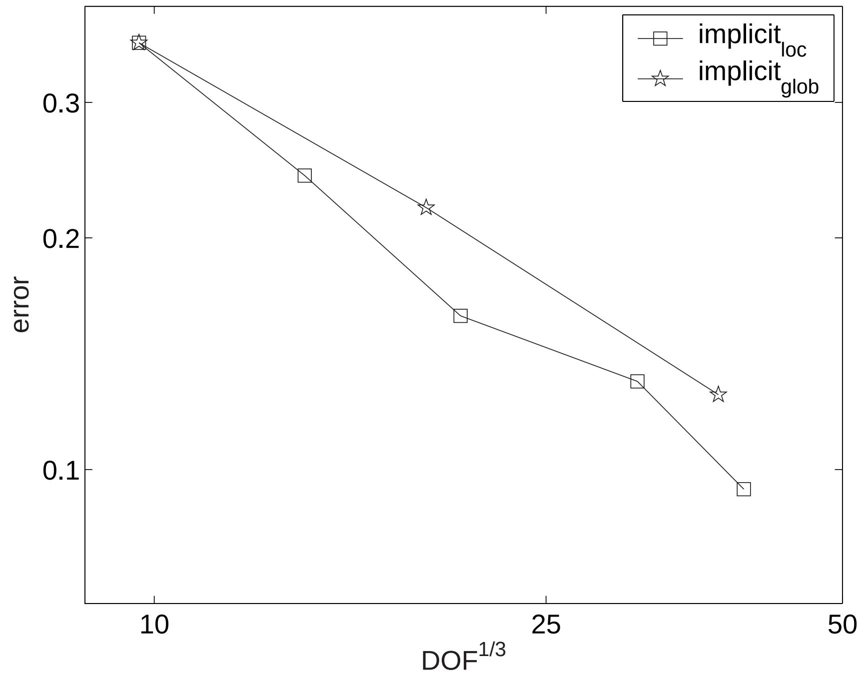

Fig. 14. Convergence plot in *loglog* scale for the Fichera cube test case with perfectly conducting boundary conditions, see Section 6.2.2.

(3.3), which will be discussed in Section 6.4.

6.3 Cylindrical domain with high wave number

It is a well known problem that for wave type equations with high wave numbers the finite element solution provides a good approximation only under certain restrictions on the finite element mesh size, see e. g. [4,5]. For more details we refer to [23] where for a range of numerical experiments the performance of a finite element scheme is demonstrated for the 1-dimensional Helmholtz equation with high wave numbers.

In this section we investigate the performance of the implicit error estimation method developed in this article for the Maxwell equations with a high wave number provided that the mesh contains a reasonable number of elements per wave length, as indicated in Lemma 7. Here we will only evaluate the performance of the implicit a posteriori error estimator. The maximum wave number attainable in a computation depends on the minimum number of elements per wave length which determines the mesh size for a given domain and is strongly influenced by the computer capacity. Moreover, for high wave number problems on fine meshes one needs to apply special techniques for the solution of the linear systems which are beyond the scope of this article.

Let us consider the same cylindrical domain as in Section 6.1.1 with the exact solution given by (6.5). The wave number is chosen to be $k = 7$ so that we have two wavelengths (λ) in the domain:

$$\lambda = \frac{2\pi}{7} \approx 0.9.$$

We will demonstrate the performance of the implicit a posteriori error estimation method on a sufficiently fine mesh and will show that the estimator is able to detect the regions with large error.

The finite element mesh, constructed for this example has 118602 tetrahedra and 146943 edges in the domain which results in an average mesh size $h = 0.12$. The solution of the Maxwell equations and the application of the implicit error estimation method on this mesh produced the following results for the implicit error estimate, analytic error, effectivity index and correlation coefficient, respectively:

$$\delta_h = 0.0974,\ \delta = 0.1619,\ \epsilon_h = 0.60,\ r = 0.71. \tag{6.6}$$

The effectivity index, correlation coefficient and the error distribution diagram, shown in Figure 15, indicate that the implicit error estimation technique is able to detect elements with a relatively large error for a wave number $k = 7$. This shows that the adaptive algorithm is also applicable for larger values of the wave number k. A further increase in wave number, however, requires computational meshes which are significantly larger than used in the test cases discussed in this section and are beyond the present capabilities of our computers.

6.4 Influence of the local basis on the implicit a posteriori error estimator

As discussed in the previous sections, an improper choice of the local basis used for the solution of (3.3) may result in a poor approximation of the exact error. We would like to mention that for some simple test cases (not described in this article) we have also implemented the implicit error estimation technique with first order Nédélec elements as a local basis for (3.3). The obtained error distribution diagrams of this implicit error estimation method did, however, not describe the true error very well. Here we discuss the performance of the implicit error estimation method on the test case described in Section 6.1.2 when using the full second order Nédélec basis [38] for the solution of (3.3). Compared to the basis used in the previous section we only add the linear part of the second order Nédélec basis functions which results in a total of 20 basis functions per element. This increases the computational work required for the implicit error estimation with $\frac{20^3}{8^3} = 15.625$ times more than for the

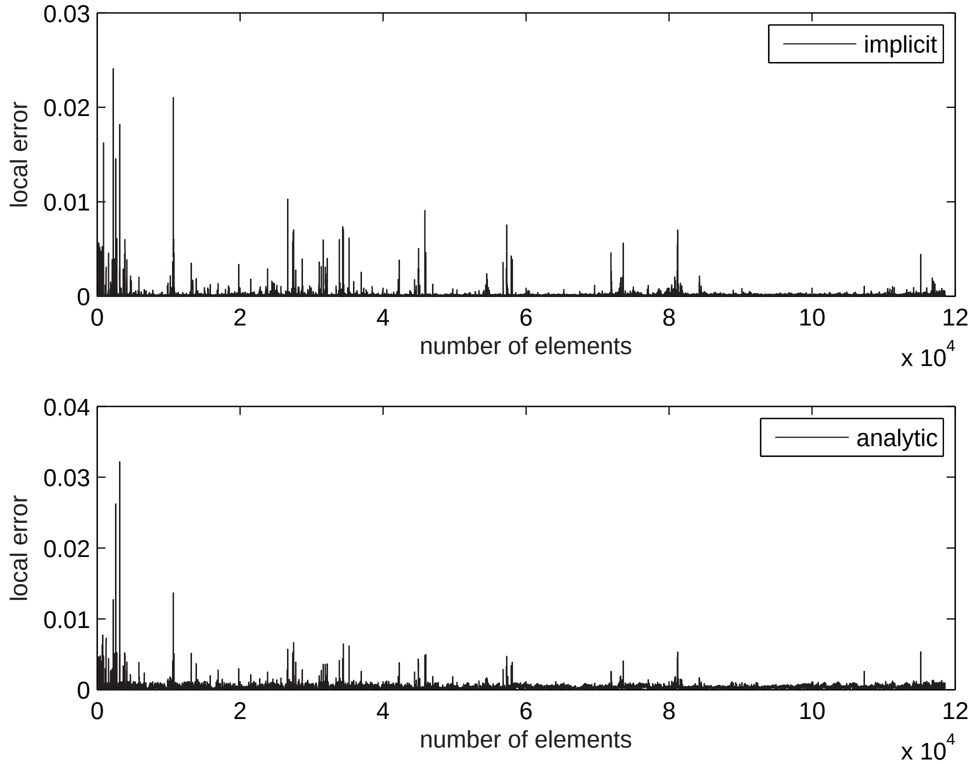

Fig. 15. Element-wise error distribution of the implicit error estimate and the exact error on the finite element mesh in the cylindrical domain with a wave number $k = 7$.

basis functions used in our experiments, but also has a negative effect on the accuracy.

In Table 6 the numerical results of the implicit error estimation using the full Nédélec second order basis in (3.3) are given.

The results from Table 6 show that the global error obtained with the implicit error estimation method is now far from the exact error which results in large numbers for the effectivity index. Moreover, on finer meshes the error of the implicit estimator does not converge, although the method produced moderate correlation coefficients. This example also shows that both the effectivity index and the correlation coefficient are important factors to judge the quality of the error estimator.

Table 6
Implicit error estimate δ_h, analytic error δ, effectivity index ε_h and correlation coefficient r on the cylindrical domain with non-homogeneous tangential boundary conditions, see Section 6.1.2. For the solution of (3.3) the full second order Nédélec basis is used.

	# edges	# elements	δ_h	δ	ε_h	r
$\mathtt{mesh}_0$	1231	981	3.3382	0.2209	15.11	0.59
$\mathtt{mesh}_1$	5219	4287	4.2651	0.1449	29.41	0.59
$\mathtt{mesh}_2$	10967	9018	4.6682	0.1156	40.38	0.65
$\mathtt{mesh}_3$	15277	12542	5.4128	0.1068	50.66	0.65
$\mathtt{mesh}_4$	26861	24853	6.0435	0.0936	64.49	0.69

7 Conclusions

We discussed an adaptive finite element method using tetrahedral Nédélec elements applied to the Maxwell equations on three-dimensional domains. The adaptation is based on an implicit error estimation technique. We show that the local problems defined for the error equation are well posed. The local problems are solved with a finite element method using second order Nédélec elements without the linear basis functions. The method is tested on various examples with non-convex domains and the results show a good prediction of the true error, both locally and globally. Based on the theoretical analysis and the numerical results we conclude that the implicit error estimation technique is a powerful method for the adaptive solution of the Maxwell equations. We have proposed a mesh adaptation algorithm and showed how it can be tuned for the Centaur mesh generation package. The algorithm creates adaptive meshes without a drastic increase in the number of elements and generates high quality meshes, with no hanging nodes and no large dihedral angles in an element.

An interesting topic for future work will be the implementation of the implicit error estimation method for the Maxwell equations with higher order Nédélec elements. In that case an important challenge will be to find a suitable well defined local basis for the error equation.

Recently the analysis of the implicit error estimator has been continued, proving that the implicit error estimation technique discussed in this article is both reliable and locally efficient. More details can be found in [26].

References

[1] M. Ainsworth. The influence and selection of subspaces for a posteriori error estimators. *Numer. Math.*, 73(4):399–418, 1996.

[2] M. Ainsworth and J. T. Oden. *A posteriori error estimation in finite element analysis*. Pure and Applied Mathematics. Wiley-Interscience [John Wiley & Sons], New York, 2000.

[3] M. Ainsworth and B. Senior. An adaptive refinement strategy for *hp*-finite element computations. In *Proceedings of the International Centre for Mathematical Sciences Conference on Grid Adaptation in Computational PDEs: Theory and Applications (Edinburgh, 1996)*, volume 26, pages 165–178, 1998.

[4] I. Babuška, F. Ihlenburg, T. Strouboulis, and S. K. Gangaraj. A posteriori error estimation for finite element solutions of Helmholtz' equation. I. The quality of local indicators and estimators. *Internat. J. Numer. Methods Engrg.*, 40(18):3443–3462, 1997.

[5] I. Babuška, F. Ihlenburg, T. Strouboulis, and S. K. Gangaraj. A posteriori error estimation for finite element solutions of Helmholtz' equation. II. Estimation of the pollution error. *Internat. J. Numer. Methods Engrg.*, 40(21):3883–3900, 1997.

[6] I. Babuška and W. C. Rheinboldt. Error estimates for adaptive finite element computations. *SIAM J. Numer. Anal.*, 15(4):736–754, 1978.

[7] I. Babuska and T. Strouboulis. *The finite element method and its reliability*. Clarendon Press, Oxford, 2001.

[8] W. Bangerth and R. Rannacher. *Adaptive finite element methods for differential equations*. Lectures in Mathematics ETH Zürich. Birkhäuser Verlag, Basel, 2003.

[9] R. Beck, R. Hiptmair, R. H. W. Hoppe, and B. Wohlmuth. Residual based a posteriori error estimators for eddy current computation. *M2AN Math. Model. Numer. Anal.*, 34(1):159–182, 2000.

[10] R. Beck, R. Hiptmair, and B. Wohlmuth. Hierarchical error estimator for eddy current computation. In *Numerical mathematics and advanced applications (Jyväskylä, 1999)*, pages 110–120. World Sci. Publishing, River Edge, NJ, 2000.

[11] M. M. Botha and D. B. Davidson. An explicit a posteriori error indicator for electromagnetic, finite element-boundary integral analysis. *IEEE Trans. Antennas and Propagation*, 53(11):3717–3725, 2005.

[12] M. M. Botha and D. B. Davidson. The implicit, element residual method for a posteriori error estimation in FE-BI analysis. *IEEE Trans. Antennas and Propagation*, 54(1):255–258, 2006.

[13] C. Carstensen. Some remarks on the history and future of averaging techniques in a posteriori finite element error analysis. *ZAMM Z. Angew. Math. Mech.*, 84(1):3–21, 2004.

[14] C. Carstensen and S. A. Funken. Fully reliable localized error control in the FEM. *SIAM J. Sci. Comput.*, 21(4):1465–1484 (electronic), 1999/00.

[15] W. Cecot, W. Rachowicz, and L. Demkowicz. An *hp*-adaptive finite element method for electromagnetics. III. A three-dimensional infinite element for Maxwell's equations. *Internat. J. Numer. Methods Engrg.*, 57(7):899–921, 2003.

[16] CentaurSoft. Web address: `http://www.centaursoft.com/`.

[17] M. Costabel, M. Dauge, and S. Nicaise. Singularities of Maxwell interface problems. *M2AN Math. Model. Numer. Anal.*, 33(3):627–649, 1999.

[18] L. Demkowicz. A posteriori error analysis for steady-state Maxwell's equations. In *Advances in adaptive computational methods in mechanics (Cachan, 1997)*, volume 47 of *Stud. Appl. Mech.*, pages 513–526. Elsevier, Amsterdam, 1998.

[19] L. Demkowicz, J. T. Oden, and T. Strouboulis. Adaptive finite elements for flow problems with moving boundaries. I. Variational principles and a posteriori estimates. *Comput. Methods Appl. Mech. Engrg.*, 46(2):217–251, 1984.

[20] A. Díaz-Morcillo, L. Nuño, J. V. Balbastre, and D. Sánchez-Hernández. Adaptive mesh refinement in electromagnetic problems. In *9th International Meshing Roundtable*, pages 147–155. Sandia National Laboratories, 2000.

[21] A. Ern and J.-L. Guermond. *Theory and practice of finite elements*. Springer-Verlag, New York, 2004.

[22] J. Gopalakrishnan and J. E. Pasciak. Overlapping Schwarz preconditioners for indefinite time harmonic Maxwell equations. *Math. Comp.*, 72(241):1–15 (electronic), 2003.

[23] F. Ihlenburg and I. Babuska. Finite element solution to the Helmholtz equation with high wave number. Part i: The *h*-version of the FEM. Technical report, Maryland University, College park, 1993. Available at `http://handle.dtic.mil/100.2/ADA277396/`.

[24] F. Izsák, D. Harutyunyan, and J. J. W. van der Vegt. *Implicit a posteriori error estimates for the Maxwell equations.* Internal report, Dept. of Appl. Math., University of Twente, Netherlands, 2007. `http://eprints.eemcs.utwente.nl/8448/`.

[25] F. Izsák, D. Harutyunyan, and J. J. W. van der Vegt. Implicit a posteriori error estimates for the Maxwell equations. *Math. Comp.*, accepted, 2007.

[26] F. Izsák and J. J. W. van der Vegt. A reliable and efficient implicit a posteriori error estimation technique for the time harmonic Maxwell equations. Internal report, Department of Applied Mathematics, University of Twente, Netherlands, 2007. http://eprints.eemcs.utwente.nl/11443/. Submitted to M2AN.

[27] P. Monk. *Finite Element Methods for Maxwell Equations.* Numerical Mathematics and Scientific Computation. Oxford University Press, Oxford, 2003.

[28] J.-C. Nédélec. Mixed finite elements in $\mathbb{R}^3$. *Numer. Math.*, 35(3):315–341, 1980.

[29] P. Neittaanmäki and S. Repin. *Reliable methods for computer simulation*, volume 33 of *Studies in Mathematics and its Applications.* Elsevier Science B.V., Amsterdam, 2004. Error control and a posteriori estimates.

[30] S. Nicaise. Edge elements on anisotropic meshes and approximation of the Maxwell equations. *SIAM J. Numer. Anal.*, 39(3):784–816 (electronic), 2001.

[31] U. Pekel and R. Lee. An a posteriori error reduction scheme for the three dimensional finite element solution of Maxwell's equations. *IEEE Trans. Microwave Theory Tech.*, 43(2):421–427, 1995.

[32] W. Rachowicz and L. Demkowicz. An *hp*-adaptive finite element method for electromagnetics. Part I: Data structure and constrained approximation. *Comput. Methods Appl. Mech. Engrg.*, 187(1-2):307–337, 2000.

[33] W. Rachowicz and L. Demkowicz. An *hp*-adaptive finite element method for electromagnetics. II. A 3D implementation. *Internat. J. Numer. Methods Engrg.*, 53(1):147–180, 2002. *p* and *hp* finite element methods: mathematics and engineering practice (St. Louis, MO, 2000).

[34] W. Rachowicz and A. Zdunek. An *hp*-adaptive finite element method for scattering problems in computational electromagnetics. *Internat. J. Numer. Methods Engrg.*, 62(9):1226–1249, 2005.

[35] B. Rivière and M. F. Wheeler. A posteriori error estimates and mesh adaptation strategy for discontinuous Galerkin methods applied to diffusion problems. Technical Report 00-10, The center for subsurface modeling, TICAM, The University of Texas at Austin, 2000. `http://www.ticam.utexas.edu/research/reports/2000.php`.

[36] G. Rodrigue and D. White. A vector finite element time-domain method for solving Maxwell's equations on unstructured hexahedral grids. *SIAM J. Sci. Comput.*, 23(3):683–706 (electronic), 2001.

[37] Y. Saad. *Iterative methods for sparse linear systems.* Society for Industrial and Applied Mathematics, Philadelphia, PA, second edition, 2003.

[38] J. S. Savage and A. F. Peterson. Higher order vector finite elements for tetrahedral cells. *IEEE Trans. Microwave Theory Tech.*, 44(6):874–879, 1996.

[39] N. Sczygiol and A. Nagórka. An *hp*-adaptive finite element method for the solidification problem based on explicit residual error. In *Proceedings of Computer Methods in Mechanics*, Wilsa, Poland, 3-6 June 2003.

[40] S. Sun and M. F. Wheeler. Mesh adaptation strategies for discontinuous Galerkin methods applied to reactive transport problems. In H.-W. Chu,

S. M, and B. Sanchez, editors, *Proceedings of the International Conference on Computing, Communication and Control Technologies*, pages 223–228, August 14-17, 2004.

[41] B. Timothy. *A posteriori error estimation and mesh adaptivity for finite volume and finite element methods*, volume 41 of *Lecture Notes in Computational Science and Engineering*. Springer-Verlag, Berlin, 2004.

[42] H. A. van der Vorst. *Iterative Krylov methods for large linear systems*. Cambridge University Press, 2003.

[43] R. Verfürth. *A Review of A Posteriori Error Estimation and Adaptive Mesh-Refinement Techniques*. Advances in Numerical Mathematics. Wiley - Teubner, Chichester - Stuttgart, 1996.

[44] Wikipedia. Correlation — Wikipedia, The Free Encyclopedia, 2007. `http://en.wikipedia.org/wiki/Correlation`.